Microfluidic Devices for Studying Early Response of Cytokine Signaling

by

Linlin YE

Master of Science, Chemical Engineering Practice, MIT, 2005
Master of Engineering, Chemical Engineering, Tsinghua University, China, 2003
Bachelor of Engineering, Chemical Engineering, Tsinghua University, China, 2001

Submitted to the Department of Chemical Engineering
in partial fulfillment of the requirements for the degree of

Doctor of Philosophy in Chemical Engineering

at the

MASSACHUSETTS INSTITUTE OF TECHNOLOGY

[June 2008]
May 2008

Author .....
Department of Chemical Engineering
May 7th, 2008

Certified by .....
Klavs F. Jensen
Warren K. Lewis Professor of Chemical Engineering
Professor of Materials Science and Engineering
Thesis Supervisor

Accepted by .....
William M. Deen
Carbon P. Dubbs Professor of Chemical Engineering
Chairman, Committee for Graduate Students

Microfluidic Devices for Studying Early Response of Cytokine Signaling

by

Linlin YE

Submitted to the Department of Chemical Engineering on May 7th, 2008,
in partial fulfillment of the requirements for the degree of
Doctor of Philosophy in Chemical Engineering

Abstract

This thesis presents the design, fabrication, and characterization of a microfluidic device integrated with cell culture, cell stimulation, and protein analysis as a single device towards an efficient and productive cell-based assay development. In particular, this thesis demonstrates the feasibility of culturing human cancer cells in microliter-volume reactors in batch and fed-batch operations, stimulating the cell under well-controlled and reproducible conditions at early stages, and detecting the protein signals with an immunocytochemical (In-Cell Western) assay.

These microfluidic devices take advantage of microfabrication techniques to create an environment suitable for cell culture, biomechanical and biochemical stimulation of cells, and protein detection and analysis. The microfluidic approach greatly reduces the amounts of samples and reagents necessary for these procedures and the required process time compared with their macroscopic counterparts. Moreover, the technique integrates unit operations, such as cell culture, stimulation, and protein analysis, in a single microchip.

The microfluidic technique presented in this thesis correlates the space in the microchannels with the biological process time (cell stimulation time). Thus, a single experiment in one microfluidic device is capable of generating a complete temporal cell response curve, which otherwise would have required multiple experiments and manual assays by standard microwells and pipetting techniques. The developed method also provides high time-resolution and reproducible data for studies of cell signaling events, especially at early stages. These cell signaling events are difficult to be investigated by conventional techniques.

The thesis reports the development not only of a cell population analysis method, but also of a single-cell detection and analysis technique to explore cell-to-cell variations. In this study, a new microscope stage holder was designed and machined, and an auto cell counting algorithm was developed for the single-cell analysis. This single-cell method provided data on cell-to-cell variations and showed that the average cell signaling profiles were consistent with those by population-based analysis. The

integration of the single-cell imaging and microfluidic method enabled measurements shows promise as a technique for exploring the cell signaling with single-cell resolutions.

Thesis Supervisor: Klavs F. Jensen
Title: Warren K. Lewis Professor of Chemical Engineering and Professor of Materials Science and Engineering

Acknowledgments

First and foremost, I would like to extend my gratitude to my thesis advisor, Professor Klavs Jensen, for giving me this wonderful opportunity to work in this research group and his guidance, wisdom, insights, and professional supports during the thesis work. His patience and encouragement carried me on through difficult times, and for his insights and suggestions helped to shape my research skills. His valuable feedback contributed greatly to this thesis. Many thanks to my committee members: Professors Daniel I.C. Wang, Charles L. Cooney, and Anthony Sinskey, for their invaluable inputs and suggestions. I also thank professors Peter Sorger for his enthusiasm and vision for cross-disciplinary research.

I would like to thank my collaborators for their contributions to the work in this thesis. Thanks to Mingsheng Zhang, in particular, for working closely together and for teaching me a lot about biological knowledge, as well as scientific presentations and writings. Many thanks to Leonidas Alexopoulos for his patience and supports, and for always backing me up and trouble-shooting together with me. Other members, Jamil El Ali, who helped me on temperature control support and gave me with very good suggestions; Suzanne Gaudet, whose support and knowledge were essential for applying the devices designed in this thesis on biology; Jay Cooley, who helped me out with microscope. These research collaborators and friends supported my thesis work in the five years of my life at MIT. I gratefully acknowledge the National Institutes of Health (P50-GM68762) for funding and the gifted staff of the MIT MTL for microfabrication support.

KFJ group is a wonderful and amazing place to work. The members of the group have contributed immensely to my personal and professional time at MIT. The group has been a source of friendships as well as good advice and collaboration. I feel a deep appreciation for the friendships from the group that have contributed to my survival at MIT: Ling, for being a good listener with sympathy and good idea; Mahmooda, for discussing and sharing different culture knowledge; Kishori, for her nice cake and willing to help; Jacob, for helping with the computer; Jian Wen, for helping me change the CO2 cylinders. I feel grateful for so many things from the group, from exchanging ideas and technical details to borrowing lab supplies, from sharing information about foods.

My time at MIT was made enjoyable in large part due to the many friends and groups that became a part of my life. I am grateful for time spent with friends: Fei, Liang, Jun, Jie, et.al..

Finally, I am grateful to be blessed with a wonderful family. Thanks my parents, my husband, and my sister, for their love, support, and encouragement through all of these years.

Table of Contents

List of Figures

List of Tables

Chapter 1. Introduction

1.1 Motivation

Cells respond to a multitude of external cues using a limited number of signaling pathways activated by plasma membrane receptors, such as G protein-coupled receptors (GPCRs) and receptor tyrosine kinases (RTKs). These pathways do not simply transmit, but process, encode and integrate internal and external signals, such as activation of the intrinsic tyrosine kinase. [1,2] Subsequent phosphorylation of multiple tyrosine or other residues transmits a biochemical message to a number of cytoplasmic proteins, triggering their mobilization to the cell surface. [2,3] The resulting cellular responses occur through complex biochemical circuits of protein interactions and covalent-modification cascades, and the specificity is determined by the temporal and spatial dynamics of downstream signaling components. Mathematical models of these processes integrate experimental data on the distinct spatial-temporal dynamics of signaling from different cellular compartments and provide new insight into the connection between external stimuli and the signaling outcome in terms of gene expression responses, phenotype response, and any others. But large sets of experimental data with the self-consistent and dynamic measures of protein activities are rare due to the cumbersome and complex nature of the experiments that are required. Our aim is to design a microfluidic technique to achieve cheaper, easier, and reliable experiments.

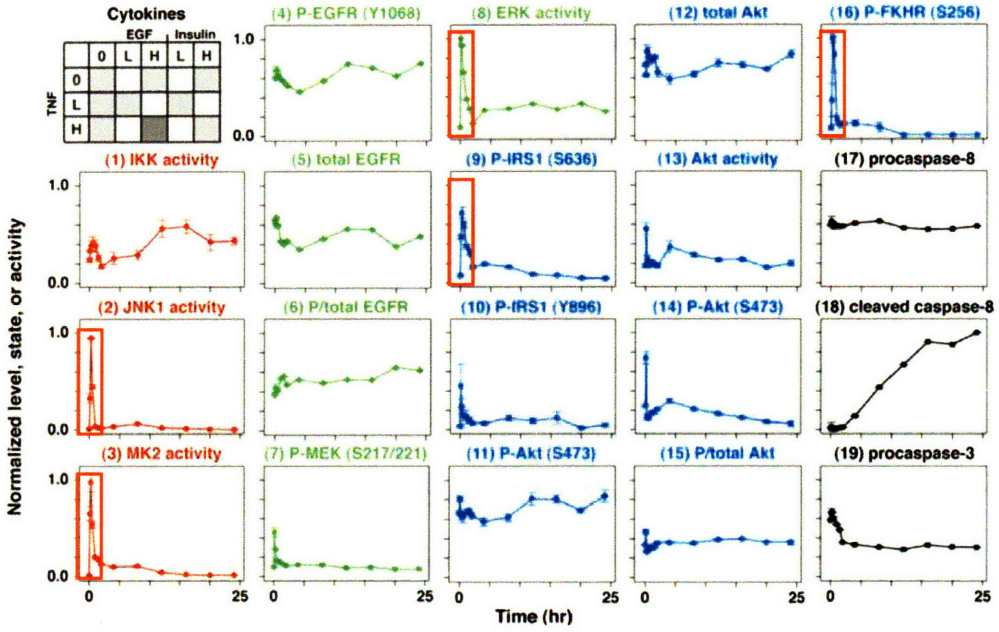

Figure 1-1. Signaling network response to 100 ng/ml TNF and 100 ng/ml EGF. [4]

Protein response events involved in cell signaling in mammalian cells can exhibit fast transient responses as illustrated in Figure 1-1. [5] Many of the cell responses show large variation in the first 5 min, but time resolution is a challenge with conventional tools. Analysis of these events requires very short treatment times and well-controlled and reproducible stimulus conditions. These pathways can be difficult to reproducibly probe with conventional laboratory techniques as even small fluctuations in the manual handling become significant at short times. Microfluidic systems offer the potential for reproducible and automated analysis with good control over experimental parameters such as temperature.

1.2 Background

1.2.1 Microfabrication for System Biology and Pharmaceuticals

Microfabricated devices are experiencing widespread growth in assays, characterization, and sensing of biological molecules and organisms. [6-8] The many benefits of such devices include small sample and reagent volumes, total integrated packages in a compact and portable size, serial processing, and eventual low production cost. [9] Methods for cell-based assays, [10] biomolecule detection [11] and separation, [12] and cell diagnosis [13] have recently been realized showing proof of principle. As such, biologically integrated microelectro-mechanical systems (BioMEMS), which include some of the previously mentioned devices, are an area of rapid growth and interest to pharmaceutical and health care industries. These are several more benefits [14] besides the general ones which have mentioned before:

- Spatial and temporal control of cell environment
- Handling low number of cells to single cells
- Continuous experiments - spatial and temporal sampling
- New techniques for sample preparation, separation, and detection
- Integration ultimately enabling new, faster experiments that could not be accomplished by conventional techniques

Microfabrication has become important to biology. The decoding of the genome [15,16] and the development of combinatorial methods of organic synthesis [17,18] have generated both therapeutic targets and drug candidates; both require microfabricated or microstructured components. Pharmaceutical and biotechnology laboratories perform thousands of assays daily, with an increasing number based on sophisticated uses of complex biochemical pathways. These assays are often carried out using small volumes of analytes and reagents and in small reaction vessels. Combinations of disease-specific genetic information and miniaturized assays are making it possible to develop new classes of diagnostic tools [19,20]. Moreover, soft lithography offers tools for micropatterning that complement and extend conventional fabrication methods. [21] Two of the key features of soft lithography are the use of elastomeric (that is, mechanically soft) materials to fabricate the pattern transfer elements by molding, and the development of techniques that pattern complex biochemicals. [22,23] Taking the advantage of microfabrication technique, integration and packaging of several functionalities into a single system is proving to be a promising task (Figure 1-2), although many cell-based microsystems available today are still in the proof-of-concept phase. [14] Typical unit operations involved in this study included cell culture, stimuli treatment, and downstream protein analysis. These functions are demonstrated in this thesis. Robust approaches to fabrication, integration and packaging remained major areas of this research. In this thesis, we design a novel high throughput microfabricated device for studying the cytokine signaling profiles induced by external stimuli treatment under short time course.

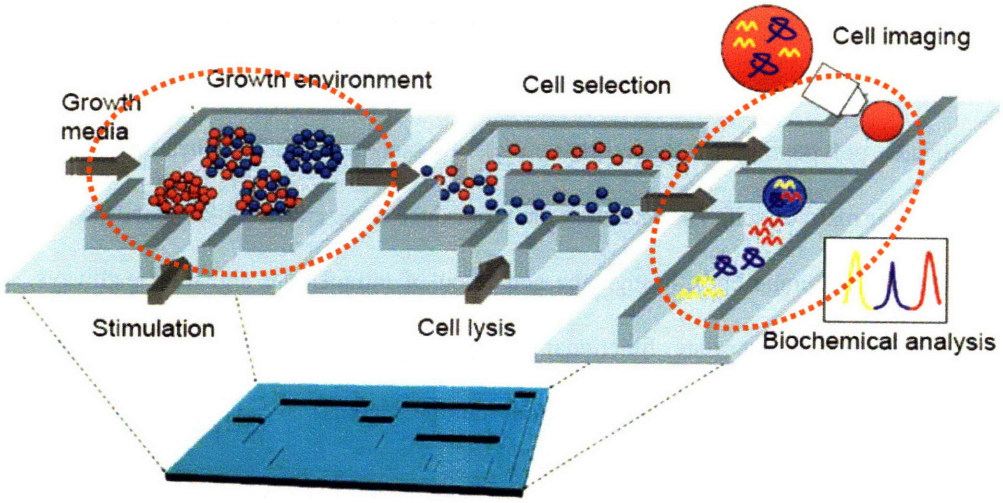

Figure 1-2. Microfabrication technique application in biological and biochemical analysis. [14]

1.2.2 Cytokine Signaling

This thesis is motivated by the fundamental system biology problem: the early cytokine signaling. Understanding of these signaling pathways is central to studies of cancer and therapy, immune responses, developmental processes, and many diseases caused by disruptions or overuse of this natural process at the cellular level. To further investigation of the early cell signaling events, it is essential to understand how cell signals are trigged, processed, and functionalized.

The ability of cells to interact with and adapt to their environment is one of the fundamental processes of cell biology. This responsiveness is achieved predominately through the expression at the cell surface of a repertoire of specific receptors that are

sensitive to the composition of the surrounding environment. The signals that trigger these receptors can be presented in a variety of contexts – for example, soluble factors (chemicals, polypeptides, protein, sugars, etc), a ligand bound to another cell, or the extracellular matrix itself. The receptors then transduce these extracellular signals across the plasma membrane and, through the activation of intracellular signaling pathways, bring about the appropriate functional response. Moreover, cells have developed sophisticated systems to integrate inputs from multiple signals.

Whether or not a cell responds to a particular cytokine depends simply on whether or not it expresses the corresponding (cognate) receptor. There are diverse families of cytokine receptors that play a key role in regulating the function of the haemtopoietic system and in coordinating immune responses. Cytokines can exert effects on numerous cell types and can interact with, induce, or inhibit other cytokines, leading to the development of the concept of a cytokine network controlling those biological processes that involve cellular interactions. [24] Cytokines can regulate diverse biological processes such as cell death and survival, cell proliferation, and cellular differentiation [25]; Moreover, different cytokines can act on the same cell type to induce a similar response. These abilities are dependent in part upon the multimeric nature of the cell receptors for cytokines, [26] but also illustrate a fundamental issue in receptor mediated signaling, the means by which diverse extracellular stimuli are integrated into a coherent responses. Here we will introduce three important cytokines which were involved in this

thesis: tumor necrosis factor (TNF), epidermal growth factor (EGF), and insulin-like growth factor (IGF).

1.1.1.1 TNF

TNF is a cytokine involved in systemic inflammation and is a member of a group of cytokines that all stimulate the acute phase reaction. The subfamily of the cell death domain containing receptors has been the focus of much recent research, stimulated by the biological important of cytokines such as TNF in the regulation of inflammatory processes. Production of and signaling induced by TNF is believed to play a key role in diseases such as rheumatoid arthritis, and a very recent clinical breakthrough has been made through the use of a soluble TNF receptor molecule to block the normal signaling induced by TNF itself. A related ligand, TRAIL, is also in clinical trials as an anticancer agent, based on the observation that its receptor appears to be expressed selectively on tumor cells. [27]

The mechanism by which this family activates downstream signal transduction has been studies extensively. The unactivated receptor is induced to trimerise by the binding of ligand, also acting as a trimmer. This trimeric receptor then recruits several signaling and adaptor molecules, collectively called the DISC complex, originally characterized for the FAS death receptor. [28] The DISC complex is then able to activate signal transduction cascades leading typically to activation of the transcription factors NF-κB and AP-1, and also in many cases to the induction of apoptosis. Serine/threonine protein kinases are key components of these intercellular pathways, and the induction of

apoptosis results from the activation of a cascade of a newly characterized family of cysteine proteases, the caspases. [29] Feedback mechanisms also operate to induce down-regulation of the receptor at the cell surface, although this process is not so well characterized. Figure 1-3 shows three of the cell signaling pathways induced by TNF. Of the three major MAPK cascades, TNF induces a strong activation of the stress-related JNK group, evokes moderate response of the p38-MAPK, and minimal activation of the classical ERKs. TRAF2 activates the JNK-inducing upstream kinases of MEKK1 and ASK1 (either directly or through GCKs and Trx, respectively), and these two kinases phosphorylate MKK, which then activates JNK. JNK translocates to the nucleus and activates transcription factors such as c-Jun and ATF. The JNK pathway is involved in cell differentiation, proliferation, and is generally pro-apoptotic. In this study, p-JNK signal was as the readout of the intercellular cell response to TNFα treatment.

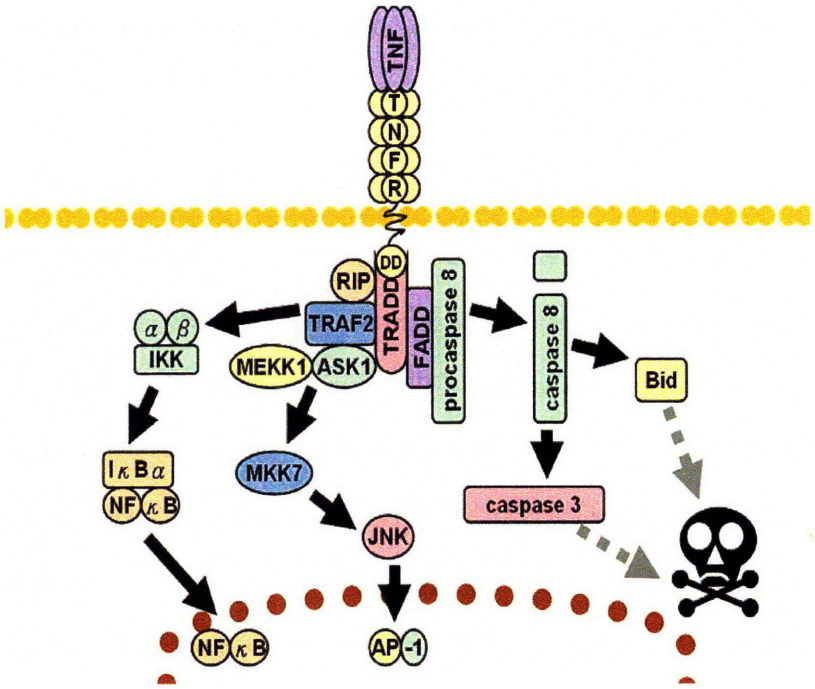

Figure 1-3. Signaling pathway of TNF receptors. Dashed grey lines represent multiple steps. [30,31]

1.1.1.2 EGF

EGF is a polypeptide growth factor, which exerts profound effects on cellular proliferation, maturation, and function, particularly during development and in the response to injury in the adult. EGF acts by binding with high affinity to epidermal growth factor receptor (EGFR) on the cell surface and stimulating the intrinsic protein-tyrosine kinase activity of the receptor. The tyrosine kinase activity in turn initiates a signal transduction cascade which results in a variety of biochemical changes within the cell - a rise in intracellular calcium levels, increased glycolysis and protein synthesis, and

increases in the expression of certain genes including the gene for EGFR - that ultimately lead to DNA synthesis and cell proliferation.[32]

The EGFR is one of the receptor-linked tyrosine kinases, which can be activated by extracellular ligands - EGF. Binding of EGF to the EGFR activates the tyrosine kinase activity of the cytoplasmic domain of the receptor. The EGFR becomes phosphorylated on tyrosines. Docking proteins such as GRB2 contain SH2 domains that bind to the phosphotyrosines of the activated receptor. [33] GRB2 binds to the guanine nucleotide exchange factor SOS. When the GRB2-SOS complex docks to phosphorylated EGFR, SOS becomes activated. [34] Activated SOS promotes the removal of GDP from Ras. Ras can then bind GTP and become active. Figure 1-4 shows one of the cell signaling pathways which is induced by EGF. Activated Ras activates the protein kinase activity of RAF kinase, [35] a serine/threonine-selective protein kinase. RAF kinase phosphorylates and activates MEK, another serine/threonine kinase. MEK phosphorylates and activates mitogen-activated protein kinase (MAPK). Such series of kinases provide opportunities for feedback regulation and signal amplification. So that when this pathway is activated, the phosphorylated MAPK signal increases with time initially, and decreases as the time duration increases. In this thesis, p-ERK signal was measured as the readout of intracellular response to EGF treatment.

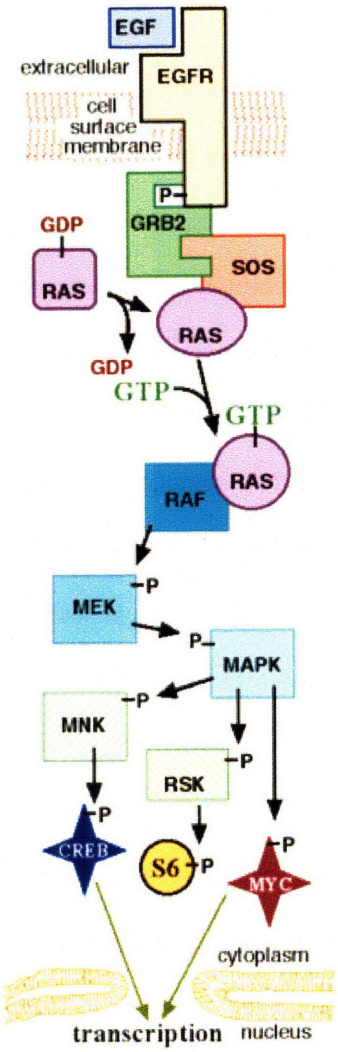

Figure 1-4. The MAPK/ERK signaling pathway of EGF receptor. [36]

1.1.1.3 IGF

IGFs are polypeptides with high sequence similarity to insulin. IGFs are part of a complex system that cells use to communicate with their physiologic environment. As the name "insulin-like growth factor" implies, IGF is structurally related to insulin, and is even capable of binding the insulin receptor, but at lower affinity than insulin. Studies of recent interest show that the Insulin/IGF plays an important role in aging. Other studies are beginning to uncover the important role the IGFs play in diseases such as cancer and diabetes, showing for instance that IGF stimulates growth of both prostate and breast cancer cells. The importance of IGFR signaling during tumor development is evident by the fact that upregulation of the IGF receptor system has been observed in many human tumors including lung [37], breast [38], and colon [39]. Epidemiological evidence suggests that elevated serum levels of IGF are considered a risk factor for the development of breast and prostate cancer in humans [40,41]. When overexpressed, IGF can provide cancer cells from many tumor types protection against a variety of chemotherapeutic and radiation therapies [42]. It has been demonstrated in many in vitro systems that increased IGFR signaling leads to increased mitogenesis, cell cycle progression, and protection against different apoptotic stresses [43,44].

Its primary action is mediated by binding to specific IGF receptors present on many cell types in many tissues. The signal is transduced by intracellular events. Several intracellular signaling pathways have been identified that are activated in response to IGF stimulation. One of them is MAPK mediated signaling pathway. It has been shown

that the ERK subgroup of MAPKs can be activated by IGF treatment via the classical receptor tyrosine kinase (RTK)/Grb2-Sos/Ras/Raf mediated pathway. [45] Activation of ERK may be partially responsible for the initial mitogenic effect of IGF. [46,47] Another IGF activated intracellular signaling pathway that has attracted much attention is mediated by phosphatidylinositol-3 kinase (PI3K). In response to IGF stimulation, activated PI3K convertsphosphatidylinositol 4, 5-bisphosohate to phosphatidylinositol 3, 4, 5-trisphosphate which results in subsequent activation of the pleckstrin homology domain (PH)-containing serine/threonine kinases PDK and Akt/PKB [48,49]. Activated PI3K also leads to activation of p70S6K, which is mediated mainly by mTOR, PDK1 and atypical PKCs [50]. IGF is one of the most potent natural activators of the AKT signaling pathway (Figure 1-5), a stimulator of cell growth and multiplication and a potent inhibitor of programmed cell death. In this thesis, p-AKT was measured as the readout of the intracellular cell response to IGF treatment.

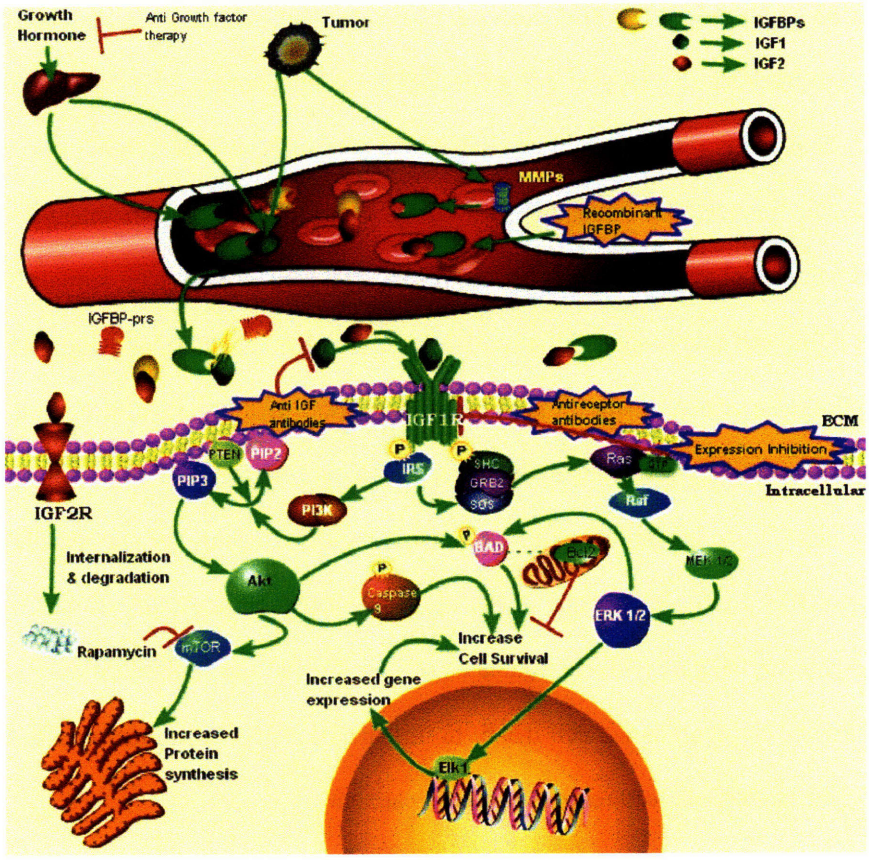

Figure 1-5. IGF pathway. [48,49]

1.3 Thesis Objective

The purpose of this thesis is to develop a high throughput technique for studying cytokine signaling of adherent cells under short stimuli treatment. The objective includes the following specific aims:

- Design and fabricate a microfluidic device for cell culture, stimuli treatment, and downstream protein analysis

- Develop in-Cell Western protocol for cell signal detection in the microfluidic devices

- Test the function of the designed microfluidic system by biological systems: to investigate the cytokine signaling of HT29 and HeLa cells treated with insulin like growth factor (IGF), EGF, TNFα.

1.4 Thesis Outline

This thesis will cover the three major categories: 1) design, fabrication, and control of the microdevices, 2) analysis methods development, 3) biological applications.

Chapter 2 describes the design, fabrication, and characterization of a microfluidic device for doing mammalian cell culture. Three different cell lines are investigated under batch reactor or semi-feed batch reactor. Two different surface coating materials and procedures are compared and finalized.

Chapter 3 presents the development of cell stimulation and downstream analysis based on population cells method and procedure. An In-Cell Western protocol in the microfluidic devices are developed and optimized. Subsequent shear assays are used to probe the cell response to their environment. Applications of the microdevices for high-throughput analysis of cell signaling of biological systems are investigated.

Chapter 4 describes capability of the microdevices to detect and measure cell signaling based on single cells. An imaging analysis method based on Matlab is developed and applied for the biological systems. The single cell analysis provided the cell variation and mean with stimulation time. It gave the same trace of the cell signaling profile as that based on the popular cell analysis.

Chapter 5 summarizes the work presented in this thesis and lists recommendations for future work.

Chapter 2. Microfluidic Devices for Adherent Cell Culture

2.1 Introduction

Cell culture is an essential tool in biological science, clinical science, and biotechnology. Conventional cell culture techniques have changed little over the last several decades and essentially consist of growing cells on a homogeneous large surface (polystyrene or glass dishes or wells) immersed in a homogeneous bath. However, in vivo cells respond to spatially and temporally organized signals in the surrounding microenvironment. Recently, microfabrication and microfluidic technologies have attracted a lot of attention in this area, with promising applications in cell-based biosensors and drug screening. [51] Microfabrication techniques offer the advantages of increased fluid control, ability to address the cellular length scale, approximating the physiologic culture environment, improved culture efficiency, and batch fabrication of high-throughput arrays. Microfluidic systems have been developed by several groups to attempt to create microenvironments of greater physiological relevance and high-throughput platforms for cell behavior analysis. [51,52] Shuler and co-workers have developed a microscale model of multi-organ interactions consisting of microfluidically connected chambers that contain mammalian cell cultures and represent ''key'' human organs, to study and predict toxicity of chemicals at the organism level. [53,54] Beebe and colleagues have manipulated and grown mouse embryos inside microfluidic elastomeric channels and observed improved and more in vivo-like development rates

compared to traditional methods.[55-58] Walker et al. have successfully cultured insect cells in microchannels for up to 7 days and showed slower growth rates than in conventional microscale cultures.[59] Takayama et al. have pioneered the use of multiple laminar streams in microfluidic channels to position [59] and sort cells, [61] to deliver biologically-active molecules to selected cell domains [62,63] and, most importantly, to stimulate signaling pathways in single cells in a physiologically-relevant way.[64] Matsue and colleagues have prepared a pattern of cardiac myocytes inside a microfluidic channel and exposed it to heterogeneous flow to demonstrate the capability of this method for high-throughput drug screening and cell toxicity studies.[65] Hung and Lee have developed a continuous perfusion microfluidic cell culture array for high-throughput cell-based assays.[66]

This thesis addresses the development of a novel microfluidic cell culture array that allows for maintaining cell cultures for one week using a batch or feed batch model, and is capable of conducting high-throughput cell-based assays. Device functionalities include the ability to maintain and monitor cells. A key aspect of the device design is to combine a sterile cell culture microenvironment, preparation of multiple assay conditions, and protein detection methods in an integrated device.

2.2 Materials and Methods

2.2.1 Microfluidic Device Fabrication and Assembly

The goal of the development of the microfluidic devices is to provide biological researchers a simple-to-use platform for adherent cell culture; specifically, the aim is to develop a single-use device that is easy to assemble and handle in any lab conditions, i.e., the replication of devices should not require clean-room conditions or expensive operations.

The microfluidic devices (Figure 2.1) were fabricated by using soft-lithography technology and replicate molding. [67] Negative master molds were fabricated out of SU-8 negative photoresist (Microchem, Newton, MA) by standard optical lithography and patterned with transparency masks drafted with AutoCAD software (Autodesk). Poly(dimethylsiloxane) (PDMS) (Sylgard 184, Dow Corning, Midland, MI) was prepared with a 10:1 ratio between the PDMS and the curing agents and molded on SU-8 master. The mold was degassed in a vacuum chamber for 30 minutes before curing in a 70℃ oven for 2 hours. The devices were then cut by a razor blade and the fluidic connection ports were punched using an 18-gauge flat-tip needle. The device was then irreversibly bonded to a coverglass/coverslip (Corning NY) after oxygen plasma treatment (PDC-32G, Harrick Scientific) on both the bottom of the device and the coverglass/coverslip. All fluidic features were 300 μm deep and 500 μm wide. PEEK tubing (1/16-in. o.d, 250-μm i.d., Upchurch Scientific) was inserted into the inlet and outlet ports and glued in place with 5-min epoxy (Devcon). With this simple fabrication

scheme, the devices become single-use devices that were disposed of after use in a biological assay.

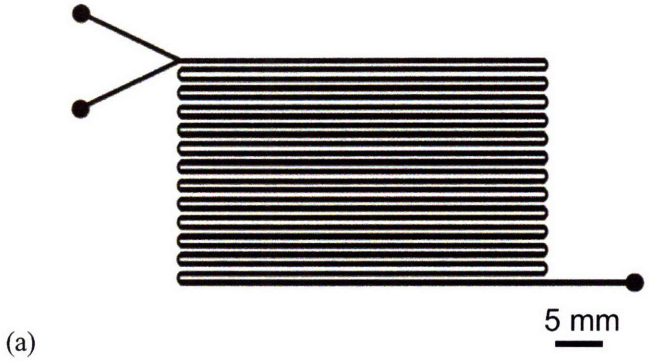

(a)

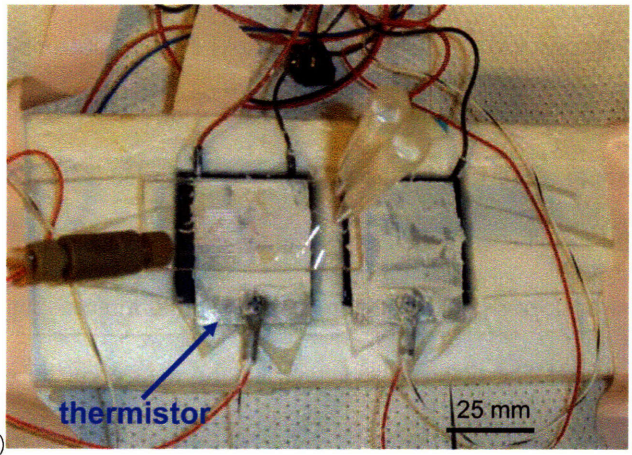

(b)

Figure 2.1. Microfluidic device for cell culture. (a) the schematic of the device; (b) the picture of the assembled microfludic device.

2.2.2 Microfluidic Device Coating

Collagen and poly-L-lysine (PLL) are common biological coating material for cell culture. Collagen can be used to coat glass for the growth of epithelial, endothelial and

muscle cells, neurons, PC12 and CHO cell lines. Type I collagen is most often used for coating substrates for cell culture because it is easily obtainable from rat tails. Nearly all types of cells adhere to the polymers of basic amino acids, such as PLL. They are particularly useful for the culture of neurons in the central nervous system. In this thesis, these two materials were chosen for coating the microfluidic devices prior to cell culture.

Two general coating procedures were explored: coating before assembly and coating after assembly.

The coating process before assembly was similar to that for patterned cell culture, as shown in Figure 2.2. Clean coverglasses/coverslips were coated with a sterile aqueous solution of 0.5 mg/mL poly-L-lysine (PLL, MW. 70,000–150,000, Sigma, MO) according to published procedures [68] or 0.8 mg/mL collagen (Type I, BD Bioscience, MA) following the procedure provided by the product sheet. Coated coverglasses/coverslips were thoroughly rinsed in sterile water for 5 times and air-dried prior to use. A small, PDMS patterning piece with the desired surface embossed patterns was placed on the PLL coated glass substrate, pressed with a stainless steel weight (100 g/cm^2), and exposed to reactive oxygen plasma using a plasma cleaner for 5 seconds–10 minutes. The surfaces of the PDMS replica and the coated glass substrate were activated with reactive oxygen plasma and brought together by visual alignment immediately after activation to form an irreversible seal. An important issue in using microfluidic devices for cell culture involves sterilizing the assembled device. Routine sterilizing processes such as UV exposure and autoclaving could not be used for the microfluidic devices

because substrates were coated with biomaterials. Therefore, in this case, the coverglasses/coverslides, PDMS, and all the connections and tubes were autoclaved before coating and assembly. All the coating procedures were done in a tissue culture hood. Prior to the seeding of the cells, the microfluidic channels were sterilized with 70 % ethanol and rinsed thoroughly with phosphaste buffered saline (PBS).

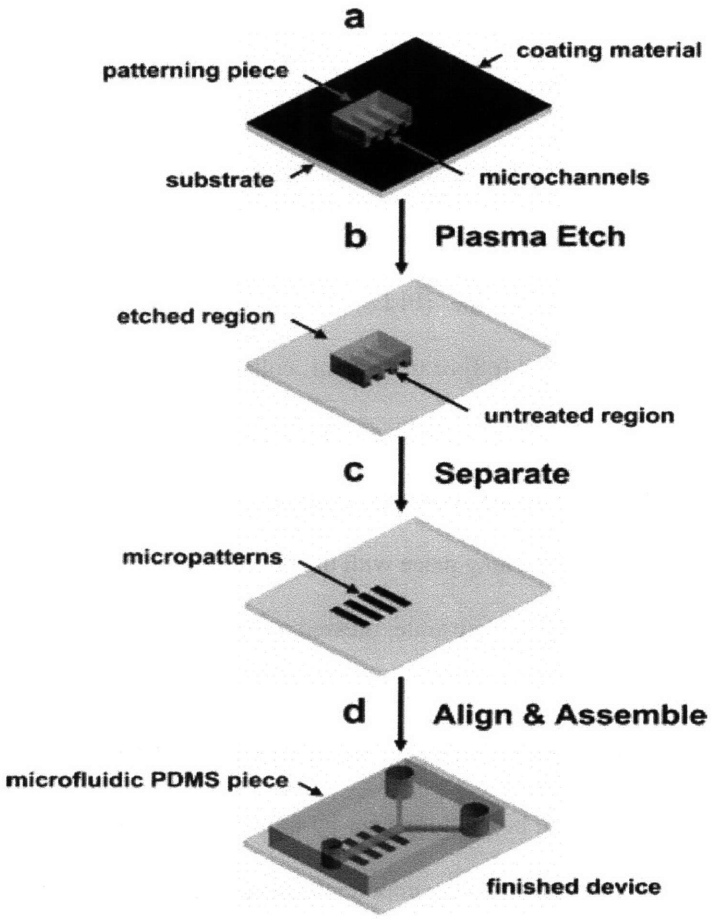

Figure 2.2. Coating procedures before assembly.

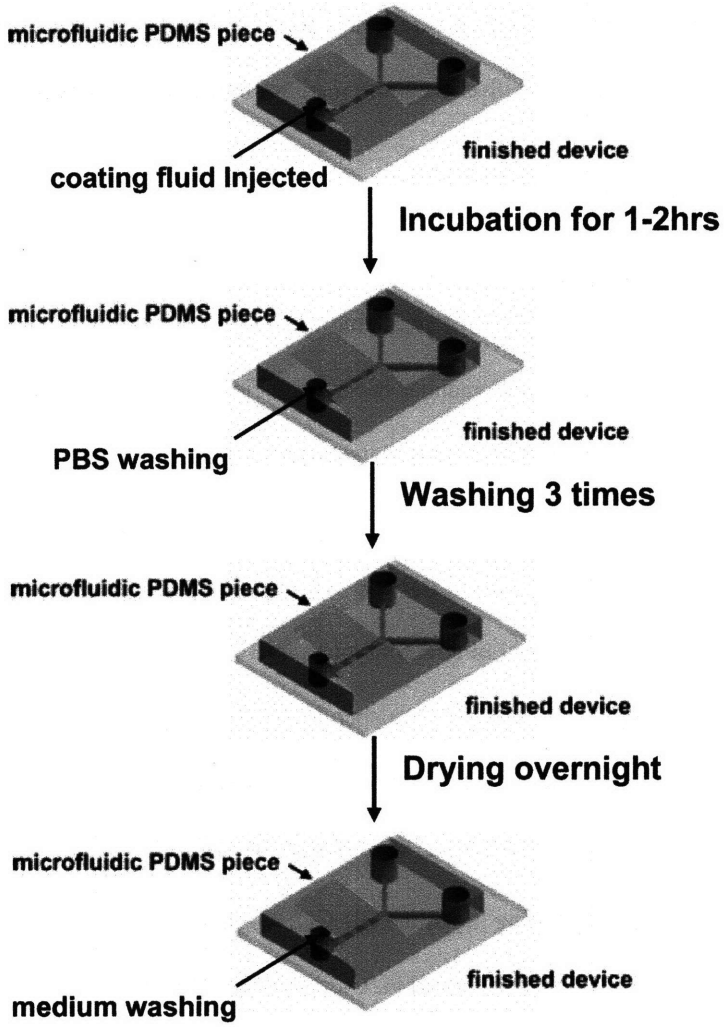

Figure 2.3. Coating procedures after assembly.

The coating process after assembly as shown in Figure 2.3 was started after autoclaving the microfluidic devices and along with flushing PLL or collagen in the microchannels, followed by physical adsorption of PLL or collagen onto the channel

surface for 2 hours at room temperature. After that, the channel was rinsed with PBS and dried overnight, followed filling with cell culture medium before cell seeding.

2.2.3 Biological Methodology

All culture components used in microfluidic devices were sterilized by autoclaving prior to use. The device was capable of maintaining a sterile environment while being continuously handled in a nonsterile manner because all fluidic connections were sealed with epoxy, isolating the microfluidic cell culture device from the outer environment. Before loading cells into microfluidic devices, HeLa cells and HT29 cells were cultured in DMEM (Sigma-Aldrich, St. Louis, MO) and McCoy's 5A (supplemented with 100 units/ml of penicillin G, 100 mg/ml of streptomycin, and 10% fetal calf serum) (GIBCO, Carlsbad, CA), respectively. The cells were suspended from culture dishes at $10^5/10^6/10^7$ cells/ml and loaded into the microfluidic culture chambers using a sterile syringe. Before introducing stimuli treatment, the device was placed inside a 37 ℃ incubator. Cell passage was achieved by flowing trypsin (GIBCO, Carlsbad, CA) into the culture chambers at the standard 0.2 % concentration. Calcein AM (Molecular Probes, Eugene, OR) was used at a final concentration of 2 μM to fluorescently label viable cells for demonstration of the cell culture functionality of the microfluidic device. The cells were cultured at 37 ℃ in a humidified incubator with 5% CO_2 in air.

2.2.4 Analytical Methods

The microfluidic devices were made by PDMS bonding to glass slides. Fluorescence and phase-contrast images were acquired through the glass slide on a Zeiss Axiovert 35 microscope with a CCD camera (SPOT, Diagnostic Instruments, Sterling Heights, MI) using commercial imaging software (OpenLab, Improvision Inc., Boston, MA). Fluorescence images were obtained in grayscale (12-bit).

2.3 Results and Discussion

2.3.1 Oxygen Supply in the Microfluidic Devices

Oxygen supply is one of the most important parameters for cell culture. In the case of PDMS microdevices for endothelial cells investigated so far [69], an oxygenator system was included in the perfusion circuit. In the present experiments, active oxygenation was not used because the high permeability of oxygen in PDMS material was sufficient as shown in the following paragraphs. The high gas permeability resulted in a simplified perfusion circuit. By rough estimation, the oxygen consumption rate $X_{O_2 consumption}$ in the present microdevice can be calculated as:

$$X_{O_2 consumption} = N_{cells/cm^2} X_{onecells} S_{device} \qquad (2\text{-}1)$$

where N_{cells/cm^2} denotes the cell density in the microdevice, $X_{onecells}$ denotes the oxygen consumption by a single cell per second, and S_{device} denotes the area for the cell culture. If we assume the cell density $N_{cells/cm^2} = 10^6 cells/cm^2$, oxygen consumption by a single cell

per second $X_{onecells} = 1\times10^{-16} mol/cell\cdot\sec$ [69] and the cell culture area $S_{device} = 0.25cm^2$ as an over-estimation, the total oxygen consumption in the device per day $X_{O_2 consumption}$ is calculated to be around $2.16\times10^{-6} mol/device/day$.

Given the permeability of oxygen in PDMS D_{PDMS} [70], the amount of oxygen that could be supplied to the device per day $F_{\max}$ can be estimated as:

$$F_{\max} \approx D_{PDMS}\frac{\Delta C}{\Delta z} \qquad (2\text{-}2)$$

in which ΔC denotes the oxygen concentration gradient across the PDMS layer, and Δz denotes the thickness of the PDMS wall of the device. Assuming $D_{PDMS} = 4.1\times10^{-5} cm^2/\sec$ [70], $\Delta C = 2.0\times10^{-7} mol\ O_2/cm^3$, and $\Delta z = 1\ mm$, $F_{\max}$ can be estimated as $7.08\times10^{-6} mol\ O_2/device/day$. According to this value, it can be concluded that a sufficient amount of oxygen can be supplied in the present microdevice with a 1-mm-thick PDMS wall to keep the cells in good condition during the culture.

2.3.2 Coating and Cell Adhesion on Varying Coated Surfaces

In order to test the coating procedures and cell adhesion on varying coated surfaces, a simple microdevice was used, as shown in Figure 2.4. The experimental results showed that the cell adherent performances were comparable in the two coating procedures. However, the coating process before assembly had some disadvantages compared with that after assembly. First, the coating procedure was more complex and the alignment of

the protection PDMS onto the channels was much more difficult and time-consuming. Second, the sterile environment in the microfludic devices was much more difficult to maintain. Third, the coating procedure before assembly left hydrophobic surfaces in the channel, which tended to create bubble problems. The channels behaved as if the devices had not been precoated. Plasma treatment of PDMS produces a hydrophilic surface, which after exposure to air for several hours or after autoclaving, tends to revert to a hydrophobic one. On the other hand, if the channels were coated after assembly, the PDMS surface was covered by PLL or Collagen and maintained the hydrophilic state all the time. The cell density was higher than that of the medium, so that the cells tended to rest on the bottom surface of the channel formed by the precoated coverglass/coverslip. The cells did not grow on the PDMS surfaces. In the following experiments, all the devices were precoated by the above procedure after assembly of the device.

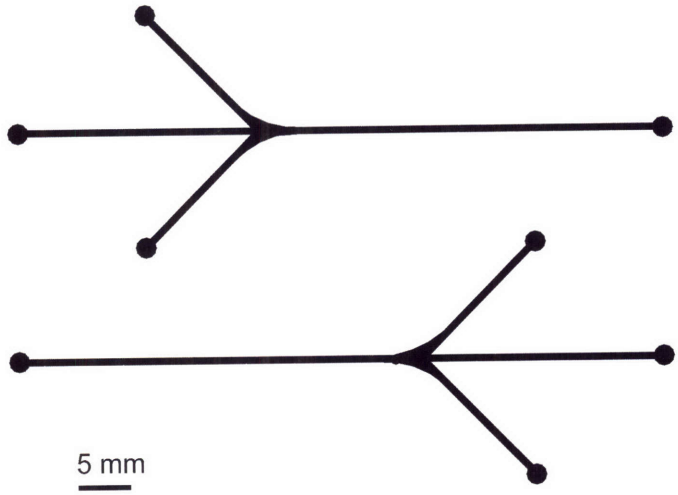

(a)

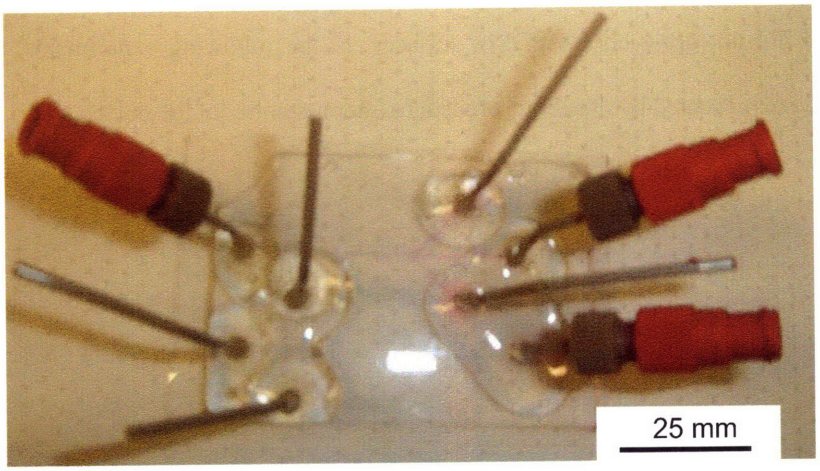

(b)

Figure 2.4. A simple microfluidic device used for surface coating tests. (a) the schematic of the microfluidic device; (b) the picture of the assembled device.

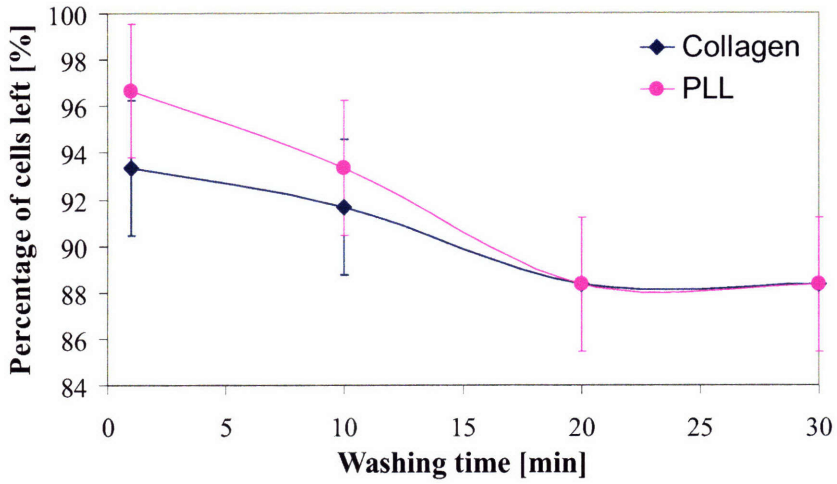

Figure 2.5. Percentage of Hela cells left on collagen and PLL coated surfaces after 1, 10, and 20 minutes of washing.

Figure 2.5 shows the percentage of the cells left on the bottom coated with collagen or PLL after washing with fresh medium of the microchannels under a flow rate of 2 μL/min controlled by a syringe pump for 1minutes, 10 minutes, 20 minutes, and 30 minutes over the cells before washing. The percentage of the cells left in the device is comparable for the two materials and around 90 – 95% after stabilization. The cell growth rate and cell viability were also comparable for the two coatings (Figure 2.5). Moreover, they corresponded to typical methods for cell culture dishes (not shown in Figure 2.6).

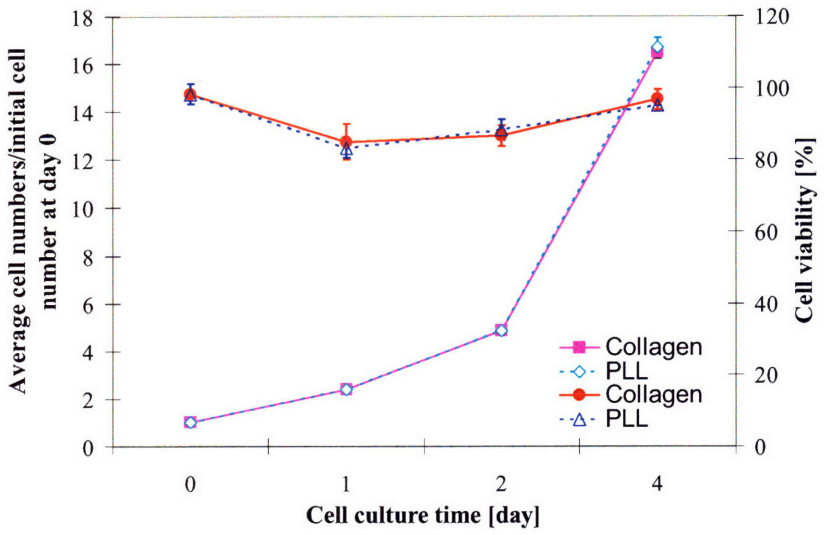

Figure 2.6. Hela cell growth rate and viability over collagen- and PLL-coated surfaces at 0, 1, 2, and 4 days after culture. The purple solid line and light blue dotted line represent the cell growth rate, and the red solid and blue dotted lines represent the cell viability.

2.3.3 Cell Culture in Microfluidic Devices

Two cell lines (Hela cells and HT29 cells) were chosen for cell culture studies in the microfluidic devices. Three initial cell concentrations of 10^5, 10^6, and 10^7 cells/mL were tested in order to evaluate suitable densities with respect to growth space, clogging, distribution, and visibility. The higher concentration resulted in relatively densely packed cells with little space in between. To enable single cell identification and ease measurements of proliferation, the concentration 10^6 cells/mL was used in the majority of the subsequent experiments. One challenge was that most of the cells did not settle to the bottom immediately after the injection was stopped but continued to flow toward the

outlet. Therefore, after the channels were closed at all the ends, the cell concentration in the channels was less than the measured loading cell concentration.

Several problems of technique had been solved for cell culture in the microfluidic devices: evaporation, bubbling, leaking, cell aggregation, sterilization, etc.

- Evaporation: Evaporation is a critical problem when handling submicroliter volumes of fluids. A common challenge with PDMS-based microfluidic chips, however, is evaporation through PDMS. Evaporation is especially detrimental to cell culture in microfluidic chips because even the slightest amount of evaporation from the small liquid volumes present in microfluidic systems results in a significant increase in osmolality. It is well-documented that elevated osmolality can affect ion balance,[71] cellular growth rate,[72] metabolism,[73,74] antibody production rate,[75] signaling,[76] and gene expression.[75,77] Therefore, in this study, the microfluidic devices were put in an enclosed box which contained steriled water in advance. This method reduced the evaporation from the device.

- Bubbling: Cell damage and destruction can be induced from bubble stress. Therefore, bubbles had to be avoided in the microchannels. Bubbles resulting from the air trapped before the process started could be eliminated by pumping carbon dioxide (CO_2) into the inner space first to expel the air. Since CO_2 dissolves in water, a minor amount of trapped CO_2 would not

create bubbles. However, it was much more difficult to eliminate bubble generated during the process when fluid filled the whole space, and especially when the bubbles attached to certain areas of the channels or chambers. One could examine the sealing of the whole system, but this could not remove any already-existing bubbles. Thus, if bubble were created, we redid the experiments.

- Leaking: It is a very common problem in microfluidic chips. By optimizing the operation parameters, leaking was minimized between the glass and PDMS, or from the inlets/outlets. If leaking happened during the experiments, the experiments had to be redone.

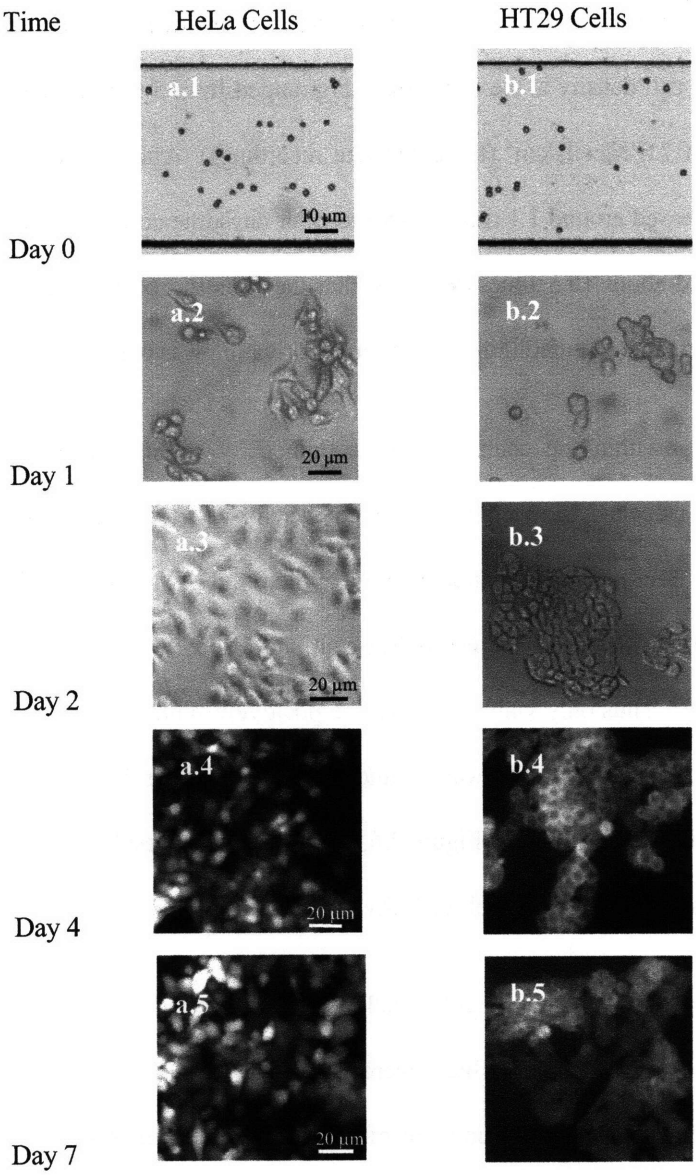

Figure 2.7. a.1-4: Hela cells cultured in the micro-devices after 0, 1, 2, and 4 days, respectively, b. 1-4: HT29 cells cultured in the micro-devices after 0, 1, 2, and 4 days, respectively.

Figure 2.7 shows the two cell lines cultured in the microfluidic devices after 0, 1, 2, and 4 days. The cell density at the very beginning ranged from 5 to 10 Mcells/cm^2, with a mean value of 7.6 Mcells/cm^2 (three separate recordings). After two days, the mean cell density increased around 1.1 times, and after four days, the corresponding mean cell density increased about 15.5 times, showing that the cells did proliferate and function within our system and that medium- to long-term cultivation was possible.

Cell viability within the channels was examined by staining the cells with the fluorescent dye calcein-AM, a commonly used dye for cell tracking. The dye is cell permeable and nonfluorescent extracellularly. When the AM group is cleaved by esterases in the cell, the dye becomes fluorescent and also cell impermeable, i.e., it is trapped in the cell. Thus only viable cells will be positively stained. As shown in Figure 2.6, on average, the cell viability was around 80 % - 95% after 1, 2, and 4 days cell growth in the microdevices. Not in Figure 2.6, the experimental results also showed that after one week of cell culture, the cell viability was also about 90 %.

Hepatocarcinoma liver cells (HepG2 cells) were also tested for cell culture in the designed mcirofluidic devices, which were grown in Eagle's Minimum Essential Medium (supplemented with 100 units/ml of penicillin G, 100 mg/ml of streptomycin, and 10% fetal calf serum) (GIBCO, Carlsbad, CA). As the HepG2 cells were growing, some waste was secreted. When the concentration of this waste achieved a critical value, the cells tended to die. Therefore, a fed-batch reactor was used. A new stream of fresh medium was injected with a syringe pump at a controlled slow flow rate of 0.1 μL/min

after 3-days cell culture. Figure 2.8 shows HepG2 cells cultured in the devices for 6 days. The cell viability is around 85% -95%.

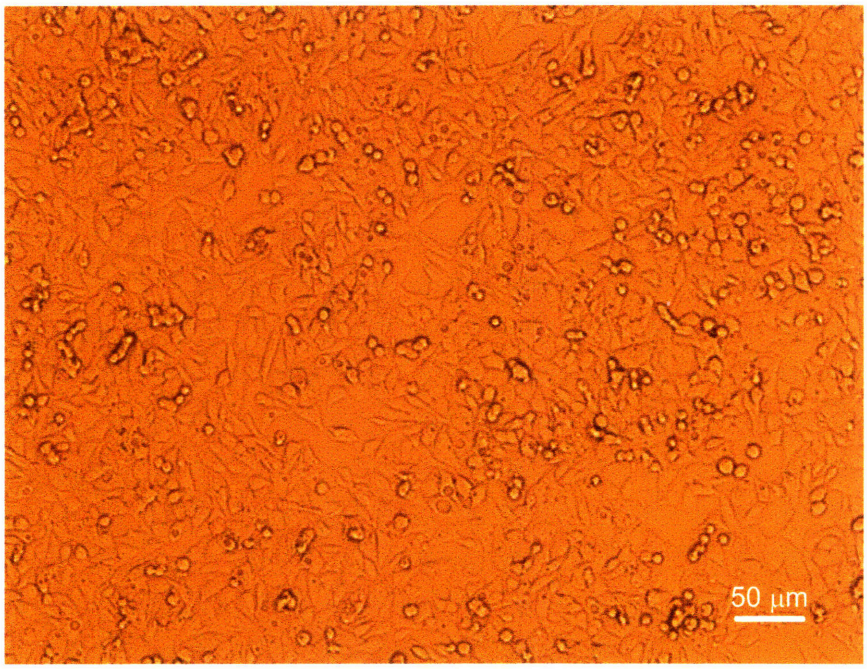

Figure 2.8. HepG2 cells cultured in the microfluidc device after 6 days.

2.4 Conclusion

Cells were alive and viable after up to 7 days of incubation within the microfluidic channels. Thus medium- to long-term cultivation and subsequent cell physiological studies will be possible. During cultivation the cell density increased 15.5 times on average after 4 days of cultivation, showing that the cells are viable and proliferate in the channels. Thus, it becomes feasible to conduct cell physiological studies in the well controlled chemical environments offered by the micorfluidic devices.

Chapter 3. Microfluidic Devices for Cytokine Signaling Study at Short Stimuli Treatment Based on Population Cells

3.1 Introduction

Major emphasis in biomedical engineering in the last decade has been placed in areas related to tissue engineering, medical diagnostics, and detection of trace amounts of biological agents. Microarray and high-throughput screening technologies are now commonly used for measuring gene and protein expression profiles and for assessing biological activity of potential drug targets [78,80]. The development of biochemical and cell biological assays [81] for screening of biomolecules, evaluating their characteristics in biological processes, and determining their pharmacological effects represents key efforts in biomedical research. PDMS-based integrated microfluidic systems [82] provide powerful platforms for integrating syntheses, bioassays, and optical measurements because of (i) rapid kinetics [83] and fast mass and heat transfer [84] within the microfluidic environment, (ii) reduced consumption of reagents, solutions, and biological samples, (iii) feasibility of integrating chemical, biological, and analytical processes on a single device, (iv) the ability to perform direct optical measurements as a result of the transparent nature of PDMS matrixes, [85] and (v) the gas permeability that allows gas exchange between enclosed microchambers and the surrounding environment [86]. Furthermore, the low elastic modulus of PDMS materials [87] permits the parallel fabrication of functional modules to perform isolation, metering, active mixing, and

trapping processes, all within a single device [88]. A number of systems have been devised that use such functional modules within microfluidic devices, including polymerase chain reaction (PCR) devices, [88] miniaturized DNA sequencers, [89] protein crystallization chambers, [90] highly integrated memory devices [91] and reaction circuits for multistep synthesis [92]. But so far no microfluidic device can explore multiple times of the biological process in a single experiment with a single device.

We demonstrate here a new type of PDMS-based microfluidic platform (Figure 3.1), in which the space in the microchannels is correlated with the biological process time. All the steps needed in stimulus-signal response analysis of signaling pathways are integrated by the use of an immunocytochemical assay (In-Cell Western), which includes cell culture, cell stimulus, cell fix, and protein analysis, into a single microchip. A single experiment in a single microfluidic device generates a complete temporal response curve, which otherwise would have required multiple experiments and manual immunocytochemical assays by standard 96-wells and pipetting techniques. The microfluidic devices are applied to explore AKT, ERK and JNK cytokine signaling in HT29 cells stimulated with IGF, EGF and TNFα for different stimulation times. This technique proves to be an efficient, productive, and high time-resolution method to study cell signaling events, especially at early stages.

3.2 Materials and Methods

3.2.1 Microfluidic Experimental Setup

A typical process flow in these experiments, as shown in Figure 3.1, started with cell culture. Prior to seeding, the device was sterilized and filled with culture media. Suspended cells were seeded at ~ 10^6 cells/mL. The cells were cultured at 37 °C in a humidified incubator with 5% CO_2 in air. After the cells were cultured in the devices after 5-6 days, starve the cells for 12 hours with a serum-free medium. After that, a fresh cell medium and stimuli to cells (cytokines or growth factors) under controlled conditions of concentration, time, and temperature were added. An air segmentation of liquid streams was used to separate the fresh medium and stimuli, and to trace the position and time of the front of the stimuli treatment. The time needed for the front of the stimuli to pass a specific position in the device and reach the end of the channel defined the stimulation time for cells in that position. Consequently, spatial positions along the channel corresponded to time points. After the stimuli, the cells were fixed instantaneously from the outlets. A primary antibody was added after 20 min, and was incubated for several hours. A fluorescently labeled second antibody was added with an additional one hour of incubation. Finally, the fluorescence was measured along the length of the channel, as shown in Figure 3.2. Each of the cell signal analysis segments along the channel included 80 – 100 pixels.

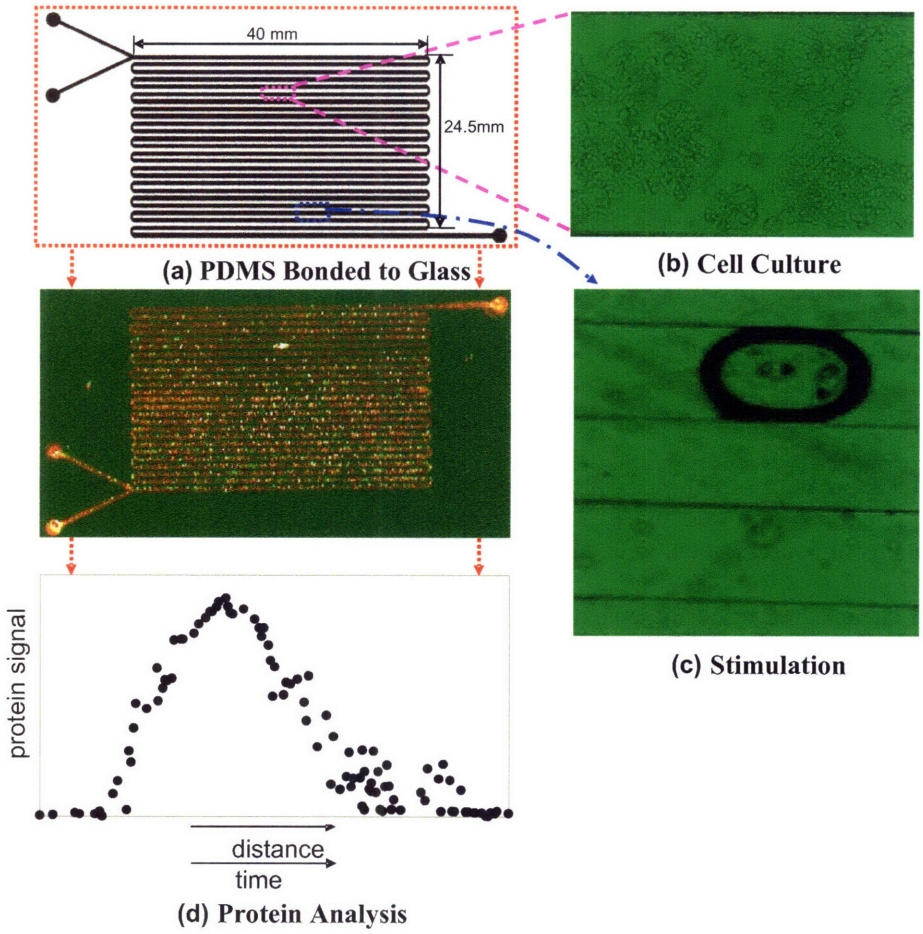

Figure 3.1. Schematic of the microfluidic system.

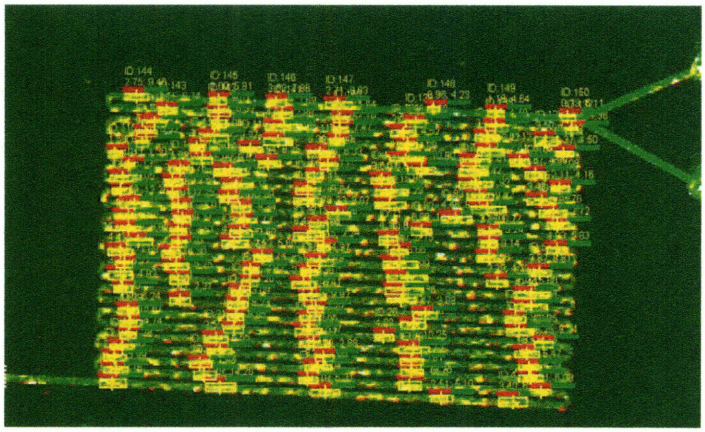

Figure 3.2. Fluorescence analysis along the microchannel by a Licor imaging system.

The desired temperature of the device during the cell stimulation and fix was achieved by a thermal control setup, as shown in Figure 3.3. TE heaters and coolers (TE-127-1.0-2.5, TE Technology Inc.) were attached to the backside of the glass slide through aluminum heat spreaders. Heat sinks were attached to the backsides of the TE modules. The temperature was regulated using proportional integral controllers (TC-24-10, TE Technology Inc.) with temperature-sensing thermistors attached to the aluminum heat spreaders providing the temperature feedback for the controllers. When the device was in the cell-stimulation stage, it was mounted on the heater side. During the fix procedure, it was moved onto the cooler side, which helped to inhibit or reduce the ongoing cell signaling transduction.

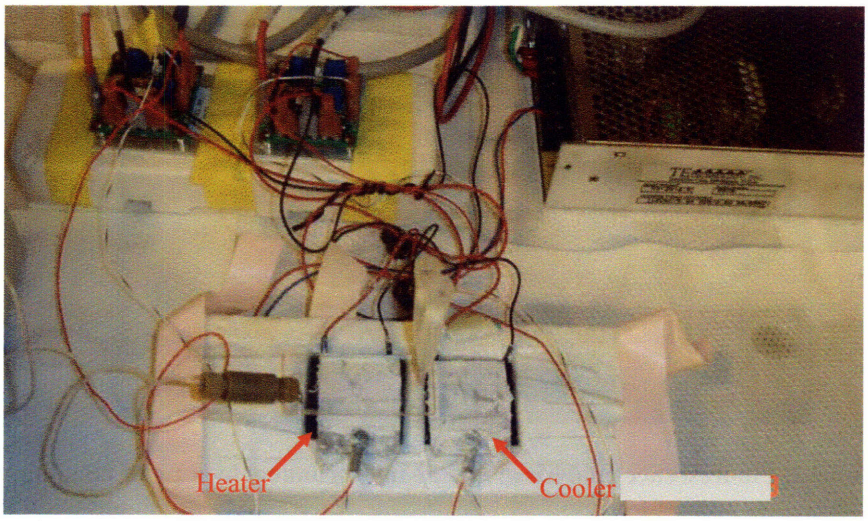

Figure 3.3. The temperature control setup for the microfludic device.

3.2.2 Microfluidic Device Fabrication and Assembly

The device was the same as the ones described in 2.2.1.

3.2.3 Biological Methodology

All culture components used in microfluidic devices were sterilized by autoclaving prior to use. The device was capable of maintaining a sterile environment while being continuously handled in a nonsterile manner because all fluidic connections were sealed with epoxy, isolating the microfluidic cell culture device from the outer environment. Before loading cells into microfluidic device, HeLa cells and HT29 cells were cultured in DMEM (Sigma-Aldrich, St. Louis, MO) and McCoy's 5A (supplemented with 100 units/ml of penicillin G, 100 mg/ml of streptomycin, and 10% fetal calf serum) (GIBCO, Carlsbad, CA), respectively. The cells were suspended from culture dishes at 10^6

cells/ml and loaded into the microfluidic culture chambers, using a sterile syringe. Before introducing stimuli treatment, the device was placed inside a 37 ℃ incubator. Cell passage was achieved by flowing trypsin (GIBCO, Carlsbad, CA) into the culture chambers at the standard 0.2 % concentration. Calcein AM (Molecular Probes, Eugene, OR) was used at a final concentration of 2 μM to fluorescently label viable cells for demonstration of the cell culture functionality of the microfluidic device. The cells were cultured at 37 ℃ in a humidified incubator with 5% CO_2 in air.

For cell signaling experiments, HT29 and HeLa cells were treated with epidermal growth factors (EGF), tumor necrosis factors-alpha (TNFα), and insulin like growth factors (IGF) at a final concentration of 100 ng/mL, 100 ng/mL, and 50 ng/mL, respectively.

3.2.4 Analytical Methods

Analysis of p-ERK, p-JNK, and p-AKT signaling was completed using an immunocytochemical assay (In-Cell Western). The principle is similar as a sandwich antibody assay (Figure 3.4). Target-specific primary antibodies are bound with the specific protein and infrared-labeled secondary antibodies are used to detect target proteins in fixed cells. The fluorescent signal is quantified. In-Cell Westerns offer broad application to the analysis of protein signaling pathways, reliable protein quantification, and cell-based determinations of IC_{50} concentrations for lead optimization. In-Cell Westerns are also a powerful tool for the study of the effects of drug components on

multiple points within one or more signaling pathway. Other traditional protein assay methods, such as Western blotting, are cumbersome and labor intensive; however, In-Cell Westerns eliminates typical Western blotting steps, such as cell lysate preparation, electrophoresis, and membrane transfer. Furthermore, high content screening methods employ very expensive complex instrumentation. In-Cell Westerns offer a practical alternative for medium to high throughput analysis.

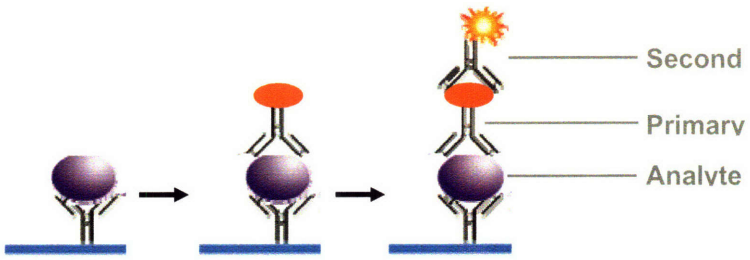

Figure 3.4. Schematic of sandwich antibody assay.

The analysis procedure was as follows. Cells were fixed after treatment in 4 % formaldehyde in PBS at room temperature for 20 minutes and washed four times with 0.1 % Triton for 5 minutes each. The cells were blocked by an Odyssey Blocking Buffer (LI-COR Biosciences, Lincoln, Nebraska) for one hour. Phospho-p38 MAP kinase (Thr180/Tyr182) antibody (1:1000) (Catalog No. 9211, Cell Signaling Technology, Danvers, MA), Phospho-SAPK/JNK (Thr183/Tyr185) antibody (1:100) (Catalog No. 9251, Cell Signaling Technology, Danvers, MA), and Phospho-Akt (Ser473) (193H12) Rabbit antibody (1:200) (Catalog No. 4058, Cell Signaling Technology, Danvers, MA) were used as primary antibodies, respectively, and added into the cells. After incubating

for several hours, the cells were washed by 0.1 mL/Channel PBS-T three times, and a second antibody (1:800 LICOR) and ToPro3 (1:2500) (Invitrogen Corporation, Carlsbad, CA) were added with an additional one hour of incubation. After washing by 0.1 mL/Channel PBS-T another three times, the fluorescence was measured along the length of the channel by a LI-COR imaging system (LI-COR Biosciences, Lincoln, Nebraska).

The LI-COR imaging system (Figure 3.5) has two detection channels. We can use one of the channels for normalization against a second target or a DNA stain. Because the difference of cell numbers can be adjusted by normalization against the DNA stain, quantification accuracy of these measurements can be maximized. Moreover, because proteins are detected in their cellular context, which eliminates variabilities and artifacts caused by cell lysis, the accuracy of the measurements by the LI-COR imaging system is enhanced and the data is more meaningful.

Figure 3.5. LI-COR imaging system.

3.3 Results and Discussion

3.3.1 Flow Effects on Primary Antibody Incubation Time

The In-Cell Western technique requires the antibodies to permeate through the cell membrane and bind with the targets. There are many more proteins in the cell than those secreted into the environment, which results in more nonspecific bindings in the cells and reduction of the binding probability with the targets. These two reasons lead to a conventional In-Cell Western protocol of over 12 hours for the primary antibody incubation. One of advantages of microfluidic devices used in this assay is a reduction of the incubation time for the antibody binding [96] because of the increased mass transfer. Figure 3.6 shows the p-AKT signal of the HT29 cells under IGF treatment by different incubation times. Under the flow condition, the cell signals measured by the florescence after half an hour or one hour incubation of the primary antibody are comparable with

those after overnight incubation without flow. In comparison, the cell signals are relatively lower after half an hour or one hour incubation of the primary antibody without flow as in the conventional method. This behavior is attributed to the mass transfer coefficient being increased by the flow in the microdevice.

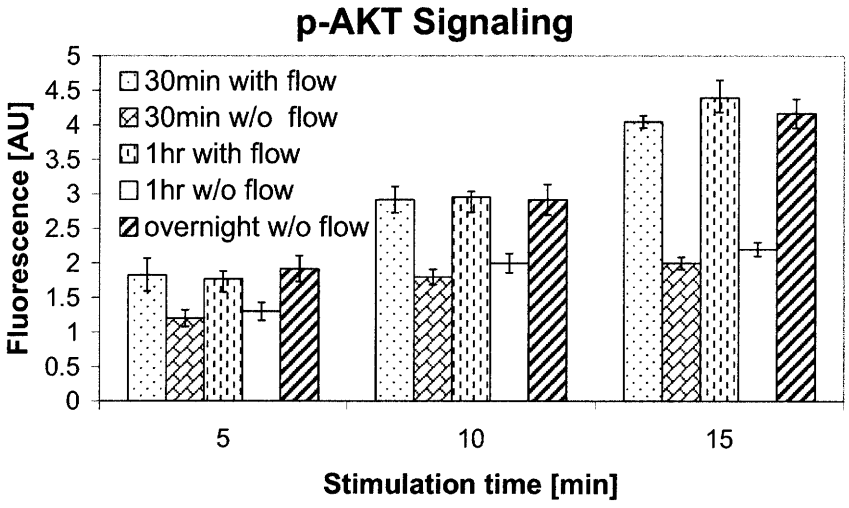

Figure 3.6. p-AKT signal of the HT29 cells under IGF treatment by different incubation times.

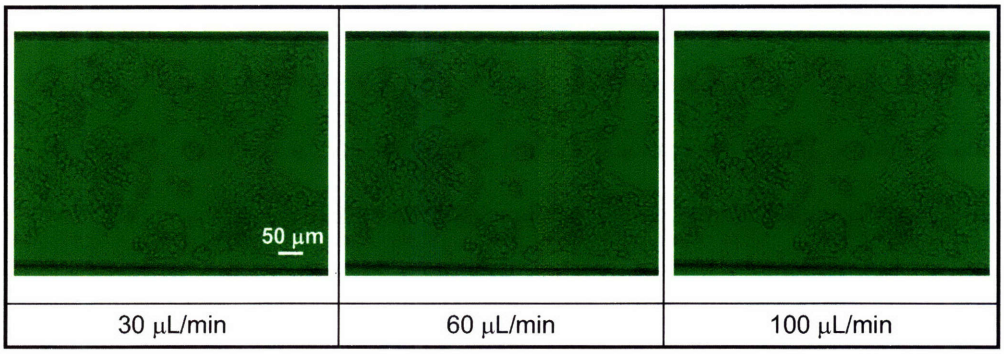

Figure 3.7. HT29 cells after continuously flowing after one hour under 30 μL/min, 60 μL/min, and 100 μL/min flow rates.

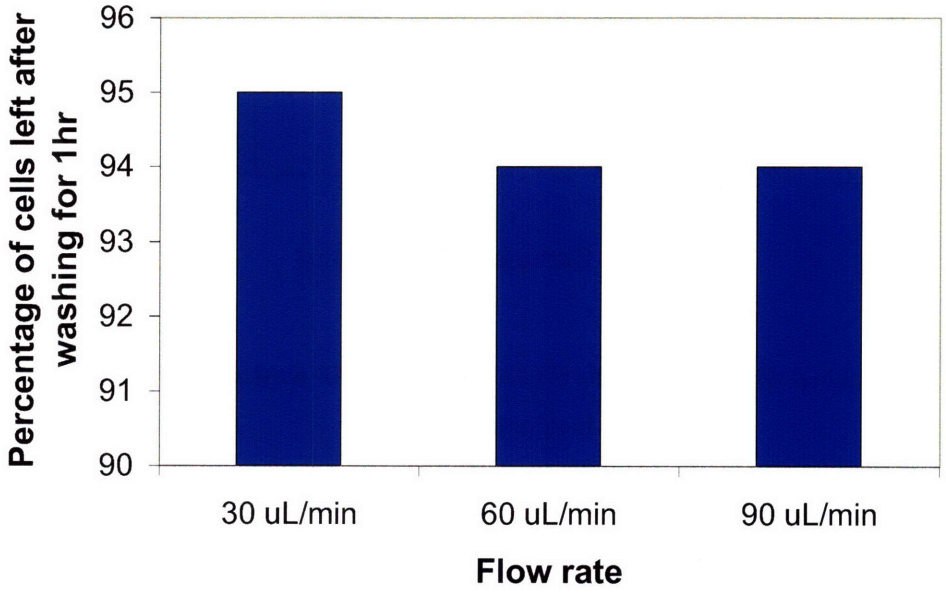

Figure 3.8. Percentage of HT29 cells left after continuously flowing after one hour under 30 μL/min, 60 μL/min, and 100 μL/min flow rates.

Another effect to be considered is whether the cells will be washed out by the flow. Figure 3.7 and Figure 3.8 show the HT29 cells after continuously flowing for 1 hour under different flow rates. The cells are not washed out by the flow and do not change their morphology under these conditions. Formaldehyde preserved cells by irreversibly cross-linking primary amino groups in proteins with other nearby nitrogen atoms in protein through a -CH2- linkage. Thus flow will not affect the protein states. A second advantage of the use of the flow for the antibody incubation is that it reduces dead cells, which helps to clear up the detection background and undesired cell signals.

3.3.2 Flow Effects on Cell Signaling Events

Our goal was to leave unstimulated cells unperturbed and stimulated cells as close as possible to cells undergoing conventional treatments for the signaling pathway analysis. Therefore, we wanted to demonstrate that the flow over the cells in the device did not in itself trigger activation of signaling pathways in cells, an important consideration for the use of the device in the analysis of signaling events. Thus, it was necessary to investigate the cellular shear stress effect on cell signaling.

Shear stress in a channel with a square cross-section of h by h is given by:

$$\tau = 6v\eta / h \qquad (3\text{-}5)$$

where τ is the shear stress (dyne/cm^2), υ is the linear flow (cm/sec), η is the viscosity of the solution (~0.0062 dyne·sec/cm^2, similar to water at 37℃). The shear stress vs. the

flow rate is plotted in Figure 3.9. The red dot represents a shear stress value with one order of magnitude smaller than typical critical shear stress value [97] which induce significant cell responses to it. The 7.5 μL/min flow rate was already significant to induce a shear stress effect on the cells for a 300 μm high channel and influence the cell signal response under stimuli treatment. Figure 3.10 shows p-AKT, p-ERK, p-JNK of HT29 cells after 10 min treatment with IGF, EGF, and TNFα under 5 μL/min and 10 μL/min flow rate. The p-AKT, p-ERK, and p-JNK signals under the high flow rate of 10 μL/min exhibit significant changes compared with those under 0 and 5 μL/min flow rates. The fluorescence intensity decreases notably. Even without any stimuli treatment, the high flow rate triggered cell response. Therefore, the flow rates to be employed in this study must be small enough not to induce significant change in cell signals.

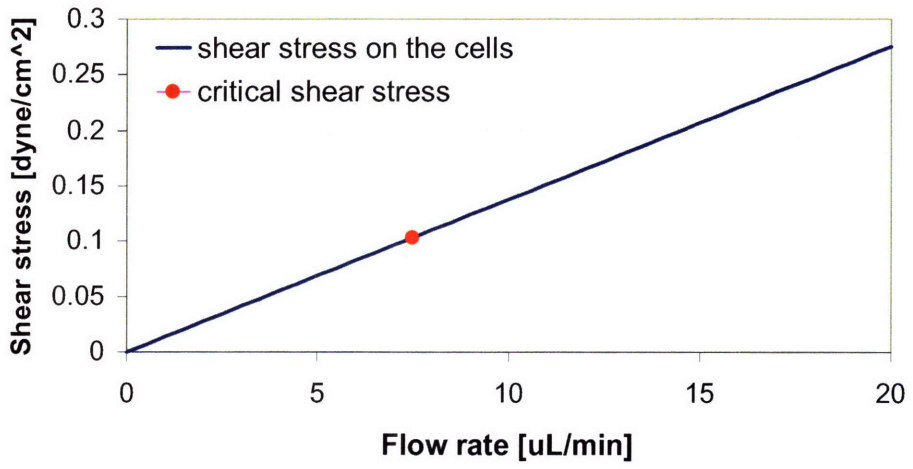

Figure 3.9. Shear stress vs. the flow rate.

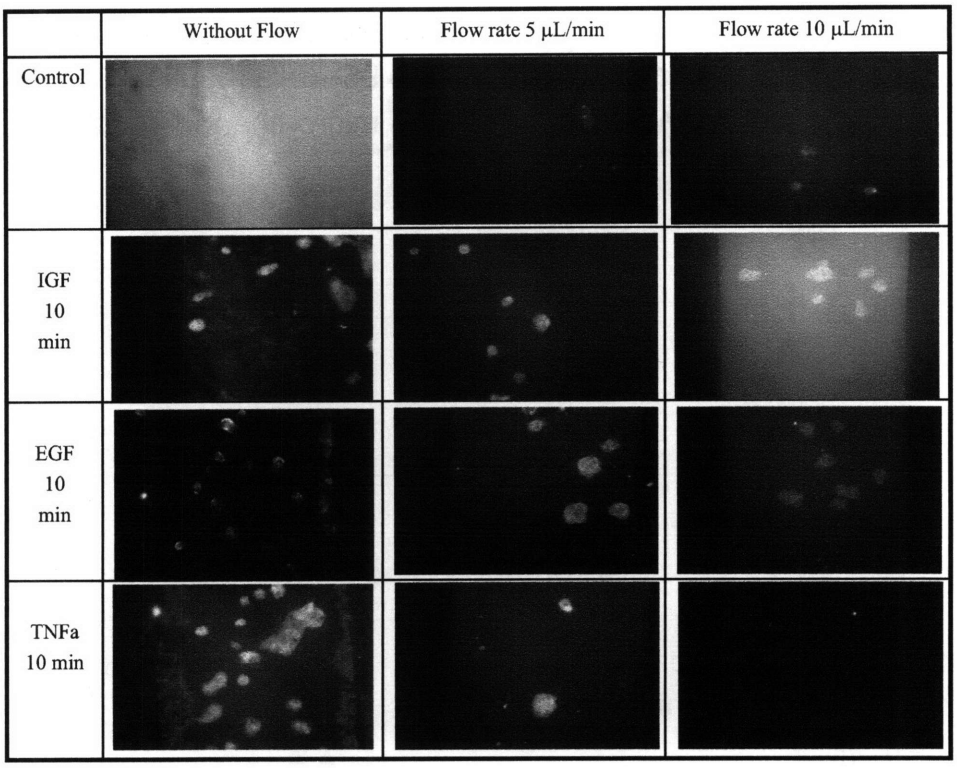

Figure 3.10. p-AKT, p-ERK, p-JNK of HT29 cells after 10 min treatment with IGF, EGF, and TNFα at no flow rate, 5 μL/min and 10 μL/min flow rates. Notice the reduced level of fluorescence and increased flow rate.

Our initial experimental results also showed (Figure 3.11) that p-JNK signaling profiles of HT29 cells and HeLa cells was shifted to the early time under 2 μL/min flow rate in the microfluidic devices compared with those completed by the conventional methods. Therefore, flow effects on cell signaling events need to be investigated.

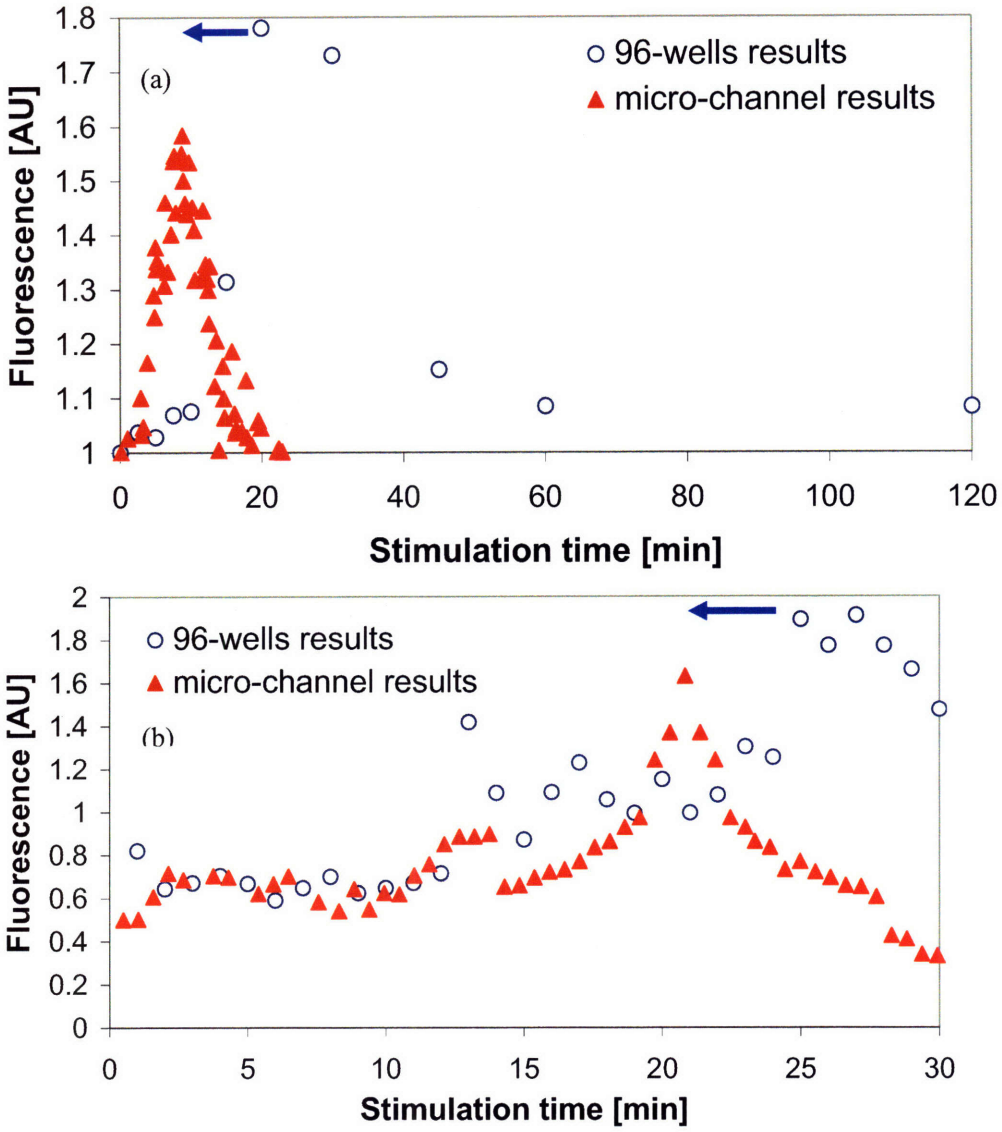

Figure 3.11. p-JNK of HT29 cells (a) and Hela cells (b) treated with TNFα under 2 μL/min flow rate in the microfluidic device and conventional 96 wells.

It has been reported that two members of MAP kinase family, ERK and JNK, are influenced by cellular shear stress. [98-101] Here, we focused on these two main signals. As shown in Figure 3.12, we found that when the flow rate was increased to 2 μL/min, p-JNK signaling profile shifted to about 15 min early, while the maximum of the signal decreased 14 %, compared to the conventional experimental results,. Increasing the flow rate to 5 μL/min, shifted the peak of the p-JNK signaling profile back about 5min, and the maximum of the signal decreased a further 3 %, compared to the results at 2 μL/min. In contrast, p-ERK signaling was not significantly affected by the flow. When the flow rate was slow (0.5 μL/min), both p-JNK and p-ERK signaling were comparable to the conventional experimental results in 96 wells. Control experiments revealed (not shown) that without treatment, at 2 μL/min and 5 μL/min flow rates, both p-JNK signaling and p-ERK signaling were similar to the profiles without any treatment under 0.5 μL/min flow (as shown in Figure 3.12). Thus the observed cell signaling outputs were not simply caused by the flow or the treatment. The performance of p-JNK signaling of HT29 cells stimulated by TNFα under different flow rate can be rationalized in the following two cofactors: inhibition induced by the shear stress and enhanced mass transfer. Cellular shear stress inhibits p-JNK signaling under TNFα treatment [100-103], reducing the peak value of the p-JNK signal. Meanwhile the increased fluid flow enhanced the mass transport to the ligand-receptor binding reaction (typically a mass transfer limited reaction). As a result, the p-JNK profile shifted to the early times at 2 μL/min or 5 μL/min compared to the profile at 0.5 μL/min. The lower peak value and

smaller shift at 5 μL/min suggest a complex interaction between the inhibition and the increased mass transfer. James Surapisitchat [100], Shila Jalali [102], and Yong-Mi Go [103], et al., have reported the high shear stress (>10 dynes/cm^2) inhibition effect on JNK, consistent with present observations, although done under low shear stress (~ 10^{-2} dynes/cm^2). Kevin Janes [104] reported that the higher the concentration of TNFα, the earlier the p-JNK signaling peaked (Figure 3.13). Figure 3.14 describes the ligand transport and binding process in the microchannel. Increasing the concentration of TNFα (C_0) or mass transfer (by increasing the flow rate) will cause a faster ligand binding response and thus a shift to earlier times as the same as the present results. Combining this effect with the known inhibition then provided an explanation for our results.

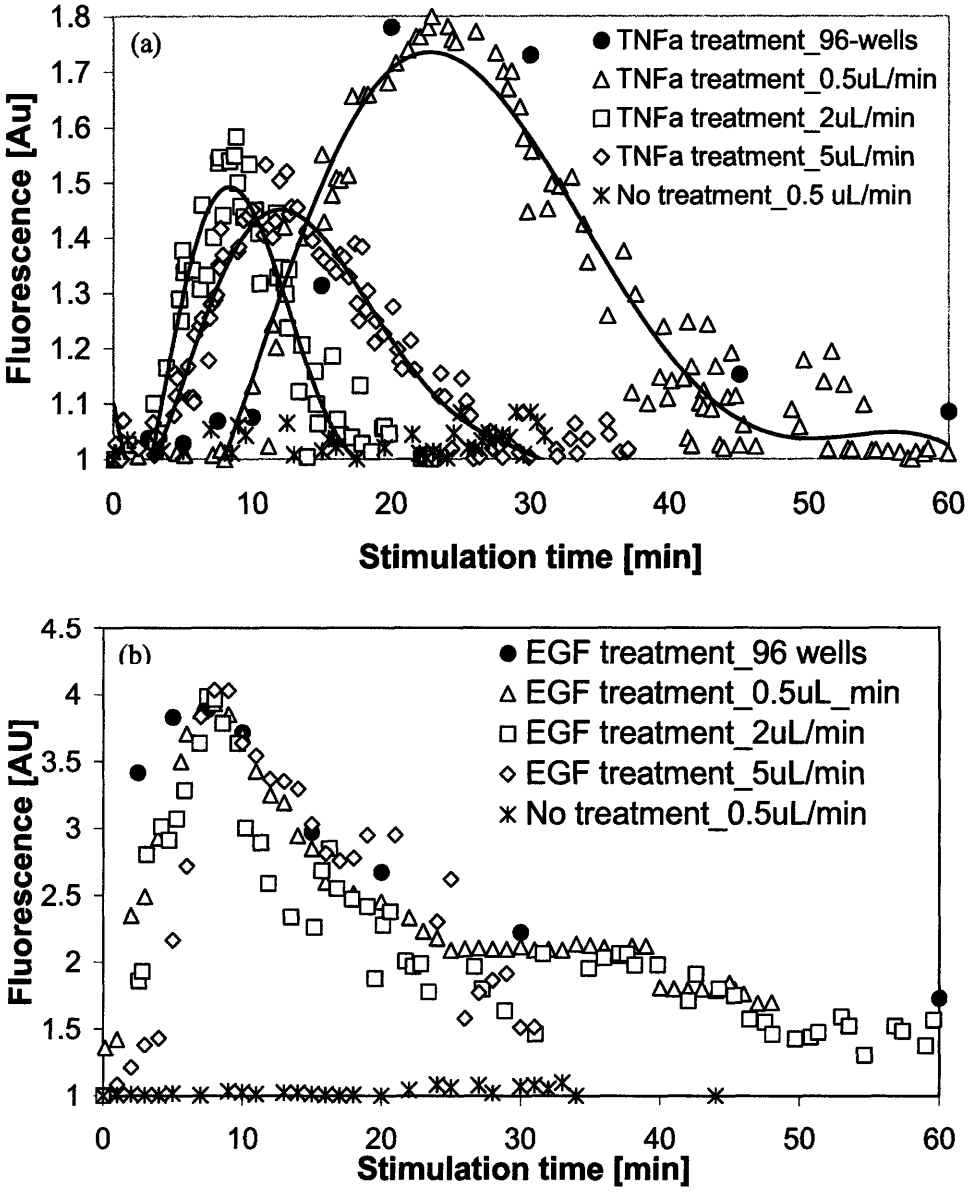

Figure 3.12. (a) Cellular shear stress effects on p-JNK signaling of HT29 cells; (b) cellular shear stress effects on p-ERK signaling of HT29 cells.

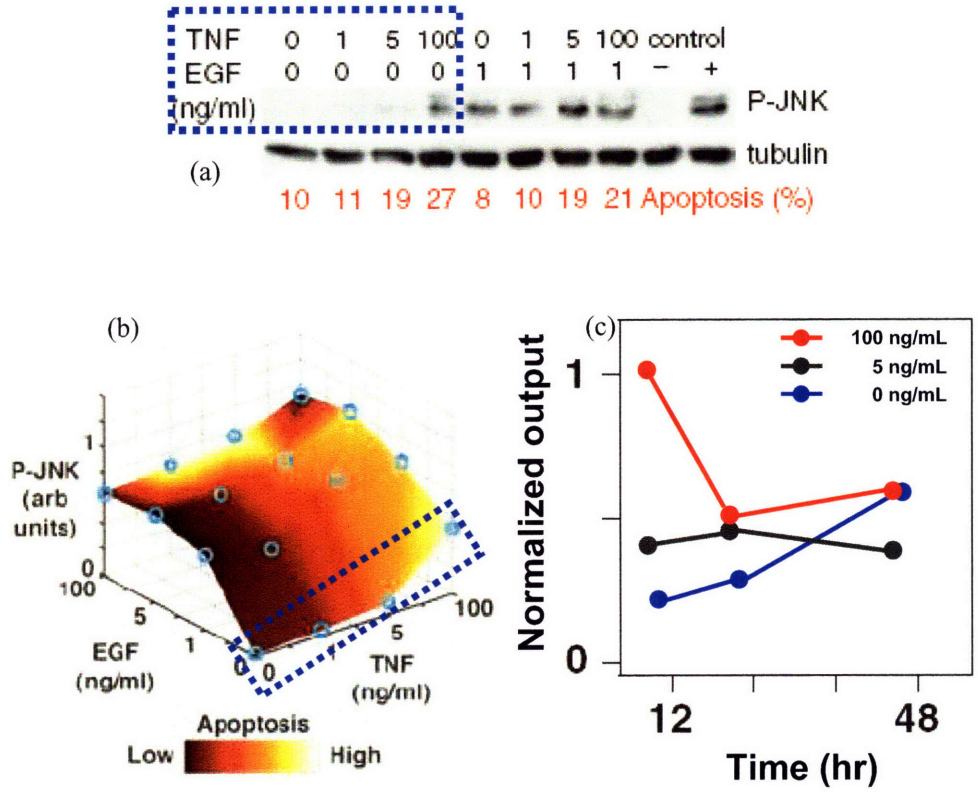

Figure 3.13. The concentration of TNFa effect on p-JNK signaling. a) JNK phosphorylation and apoptosis in HT29 cells treated with TNF, EGF, or both. P-JNK was analyzed at 15 min; b) Response surface for p-JNK (z axis) and apoptosis (color bar) induced by the input described in A); c) p-JNK signaling of HT29 cells under different concentration of TNFα. [114]

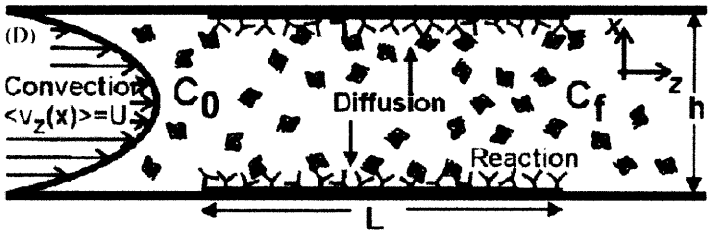

Figure 3.14. Ligand transport and binding process in the microchannel.

The lack of shear sensitivity of p-ERK signaling is also consistent with reported observations. Recent studies reported that G protein-dependent were very important in the mechanically sensitive activation of ERK and JNK signaling. [105,109] Young-Mi Go reported that one of the G protein-dependent forms, PI3Kγ, was demonstrated to be activated over a relatively short and transient time course by the shear stress stimulation. [105,109] There was no force dependency of the maximal activation of PI3Kγ. Moreover the activation of JNK signaling in response to shear stress displayed the same mechanical sensitivity as that of PI3Kγ. [110,111] In contrast, the activation of ERK by shear stress, which was not regulated by PI3Kγ, required a much higher level of shear force (10 dyn/cm^2) for its maximal activation. In this thesis, the shear stress was two or three orders of magnitude lower than 10 dyn/cm^2. Thus, p-ERK was lack of shear sensitivity in this study. [111] Selectively engagement of upstream signaling molecules such as PI3Kγ was likely to be critical to the mechanisms underlying these differential shear stress sensitivities displayed by ERK and JNK signaling pathways, although they are not determined currently. There were another research showing that the activation of

ERK by the cytokines was unaffected by the flow, but the flow inhibited the TNFα activation of JNK specifically. [112] It was suggested that the inhibitory effect of flow was not because of alterations in binding of TNFα to the receptors, but due to inhibition of a downstream mediator. The important differences in the upstream pathways stimulated by the flow leaded to the activation of different MAPKs. Therefore, we found the differential performance of p-JNK and p-ERK signaling under flow conditions.

Shear stress is the tangential component of hemodynamic forces acting on the vessel wall and constitutes a risk factor of cardiovascular diseases. [113] It is important and valuable to study the shear stress effect.

Figure 3.12 also showed that without TNFα and EGF treatment, 0.5 μL/min flow rate did not trigger the activation of JNK and ERK signaling.

3.3.3 Cytokine Signaling of HeLa and HT29 Cells Measured in the Microfluidic Devices

A series of viability and cell signaling analysis tests were conducted. It was found under 0.5 μL/min flow rate, the cell signaling behavior was not affected by the flow. Figure 3.15 showed the In-Cell Western results of p-AKT, p-ERK, and p-JNK signaling in HT29 cells stimulated with IGF, EGF and TNFα for different times in the microfluidic devices and 96-wells. Each time point was got from six parallel experiments. Stimulation of cells performed in the device resulted in pathway activation was comparable to that

using conventional methods. The error bars of the microfluidic results were relatively smaller than those of the conventional method at early times, indicating that microfuidic provided better time control in the device resulted in reproducible analysis of fast transient responses in the cell signaling pathways. Furthermore, more information in the early stage of the cell signaling responses was achieved by the microfluidic technique.

HT29 cells were studies for the early cytokine responses under short stimuli-treatment time. Three different patterns of protein profiles were measured. The p-AKT signaling increased smoothly to achieve the peak within 15 min, and then decreased to a stable signaling level which was higher than the initial value. The p-ERK signaling increased sharply, arrived the peak within 8-9 min, and then decreased slowly to a stable signaling base line which was also higher than the initial value. However, p-JNK signaling didn't changed much at the first 10 min, but after that it increased smoothly to the peak around 25 min, and then it decreased at a compared rate as the signaling increasing rate to the initial signaling level. The experimental results showed that the p-AKT, p-ERK, and p-JNK signaling stimulated with IGF, EGF, and TNFα in the microfluidic device were comparable with those from the conventional method. However, the single microfluidic device produced a complete temporal response curve in a single experiment, while the conventional approaches would have required multiple experiments and manual immunocytochemical assays by standard 96 well and pipetting techniques. Thus the microfluidic method proved to be more efficient while also providing increased time resolution – especially in the early stages of the cell signaling.

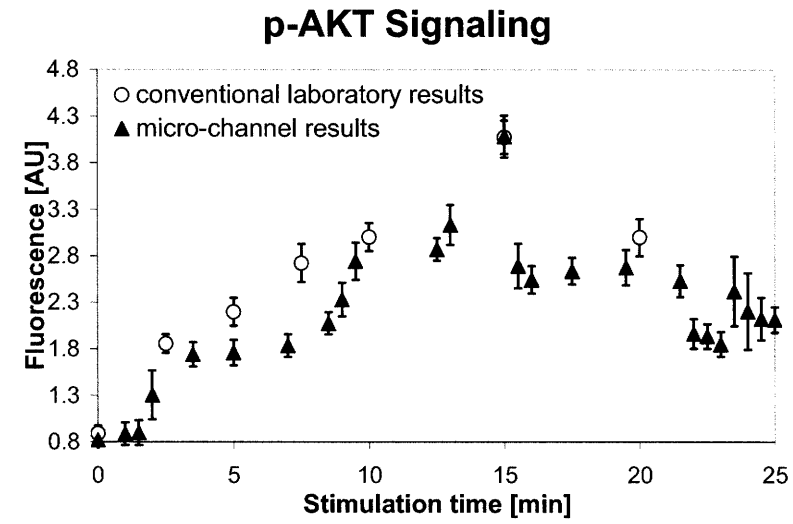
p-AKT Signaling
○ conventional laboratory results
▲ micro-channel results
Fluorescence [AU]
4.8
4.3
3.8
3.3
2.8
2.3
1.8
1.3
0.8
0
5
10
15
20
25
Stimulation time [min]

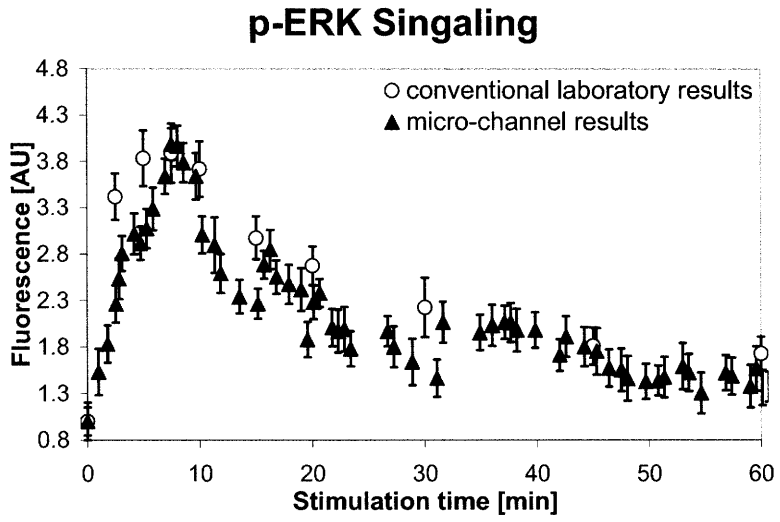
p-ERK Singaling
○ conventional laboratory results
▲ micro-channel results
Fluorescence [AU]
4.8
4.3
3.8
3.3
2.8
2.3
1.8
1.3
0.8
0
10
20
30
40
50
60
Stimulation time [min]

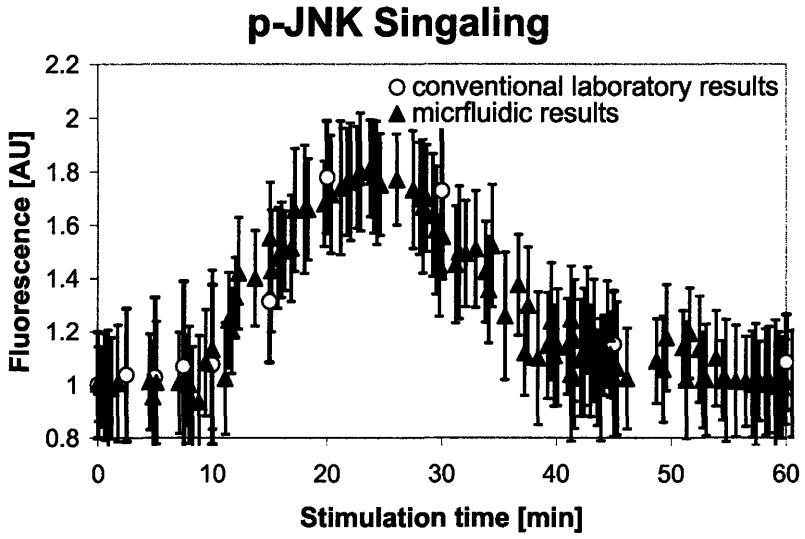

Figure 3.15. In-Cell Western results of p-AKT, p-ERK, and p-JNK signaling in HT29 stimulated with IGF, EGF and TNFα for different times in the microfluidic devices and 96-wells.

HeLa cells were tested as another biological model system. The p-AKT and p-ERK signaling stimulated with IGF and EGF in the microfluidic device were measured, as showed in Figure 3.16. These results were also comparable with those from conventional method.

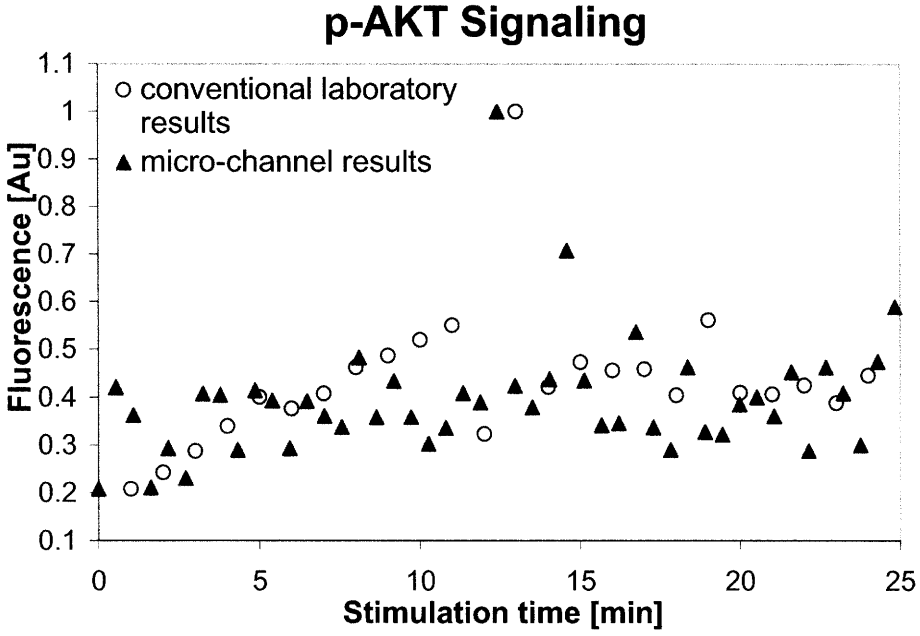
p-AKT Signaling
conventional laboratory results
micro-channel results
Fluorescence [Au]
1.1
1
0.9
0.8
0.7
0.6
0.5
0.4
0.3
0.2
0.1
0
5
10
15
20
25
Stimulation time [min]

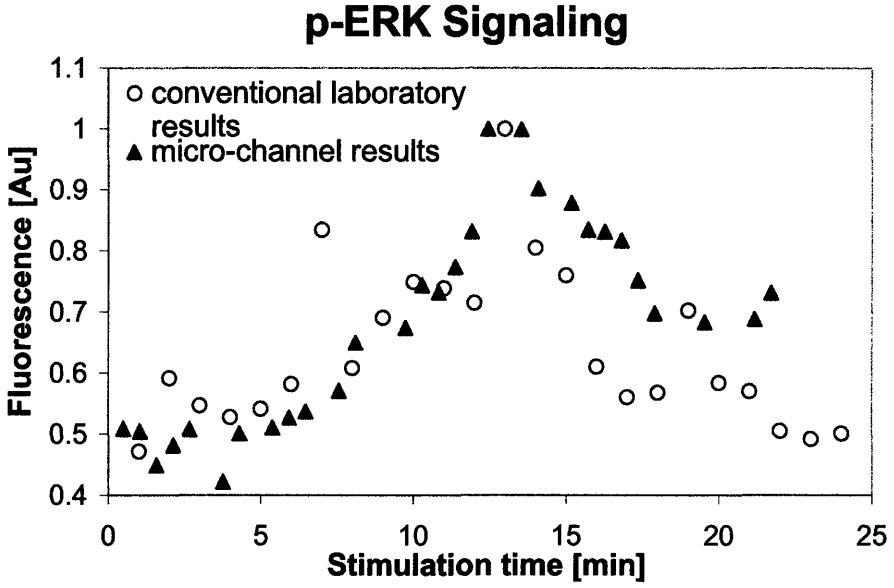

Figure 3.16. In-Cell Western results of p-AKT and p-ERK signaling in HeLa stimulated with IGF and EGF for different times in the microfluidic devices and 96-wells.

3.4 Conclusion

The designed microfluidic platform integrated cell culture, stimulation, and protein analysis in a single device. A high-throughput technique (multiple time points in a single device) was developed to study the cytokine signaling events in the early stimulation period. HT29 cells and HeLa cells were studies as the biological model systems. Three different patterns of protein profile were measured. The p-AKT, p-ERK, and p-JNK signaling stimulated with IGF, EGF, and TNFα in the microfluidic device were

comparable with those from conventional methods. This method was proved to be a efficient and productive technique for studying the transient cell signaling profile.

Chapter 4. Microfluidic Devices for Cytokine Signaling Study at Short Stimuli Treatment Based on Single Cells

4.1 Introduction

The use of modern high-throughput biotechnology (arrays, proteomics, high-speed cell sorting) has illuminated many aspects of biology including advancing our knowledge of the repertoire of cellular responses, and defining the activation of cytokine secretion. All of these techniques clearly are very useful for characterizing the spectrum of possible cellular responses; however, they do so by averaging the response of a population of cells. While it long has been known that many cells exhibit differential cellular responses, this was attributed in part to the variation in the cells present in samples. However, cells of apparently the same genotype, such as cloned and sub-cloned cell lines, also exhibit differential cellular responses and the extent of this variation has been as large as that the authors seemed prepared to examine the phenomenon. [115-120] By obscuring cell-cell variability, these measurements severely compromise our ability to decipher the regulatory mechanisms underlying the observed responses. We require new tools to permit the affordable collection of data with the dense time sampling required to capture the dynamics of cellular behavior at the population level, and to observe, and measure cellular behavior at the single cell level. In Chapter 3, cell signaling analysis based on cell population in microfluidic devices was described. In this chapter, a single cell detection and analysis technique in the microfluidic devices is

explored. Cell-to-cell variations under the same stimulation time are investigated with a high resolution microscope to measure the fluorescence intensities of the labeled proteins in the cells in each image taken along the microchannels.

4.2 Materials and Methods

4.2.1 Microfluidic Experimental Procedure

A typical process flow in these experiments was similar to that stated in 3.2, as shown in Figure 4.1, started with cell culture. Prior to seeding, the device was sterilized and filled with a culture media. Suspended cells were seeded at a cell concentration of $\sim 10^6$ cells/mL. The cells were cultured at 37 °C in a humidified incubator with 5% CO_2 in air. After the cells were cultured in the devices for 5-6 days, the cells were starved for 12 hours with a serum-free medium. After that, a fresh cell medium and stimuli to cells (cytokines or growth factors) under controlled conditions of concentration, time, and temperature were added. An air segmentation of liquid streams was used to separate the fresh medium and the stimuli, and to trace the position and time of the front of the stimuli treatment. The time needed for the front of the stimuli to pass a specific position in the device and reach the end of the channel defined the stimulation time for cells in that position. Consequently, spatial positions along the channel corresponded to time points. After the stimuli, the cells were fixed instantaneously from the outlets. A primary antibody was added after 20 min, and was incubated for several hours. A fluorescently labeled second antibody was added with an additional one hour of incubation. Finally, the fluorescence was measured along the length of the channel by microscope, as shown

in Figure 4.2. Each of the cell signal analysis segments along the channel included 100-200 cells.

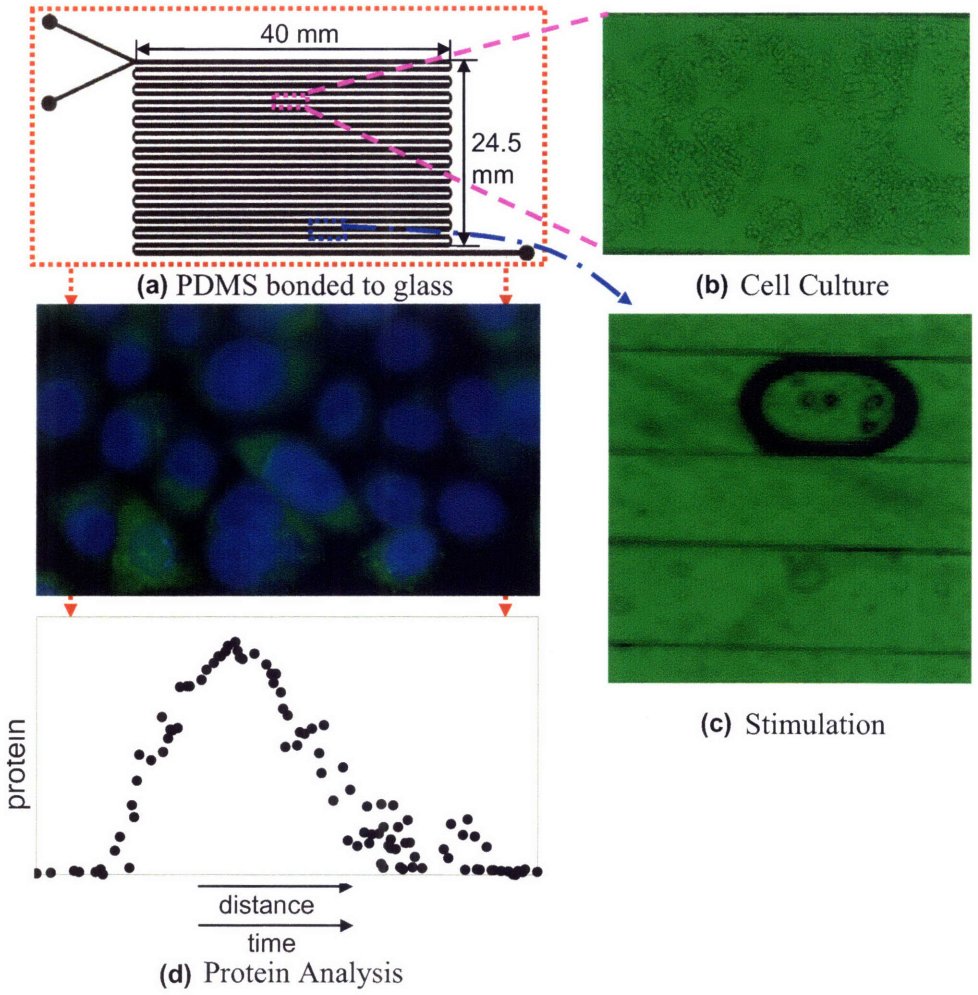

Figure 4.1. Schematic of Microfluidic System.

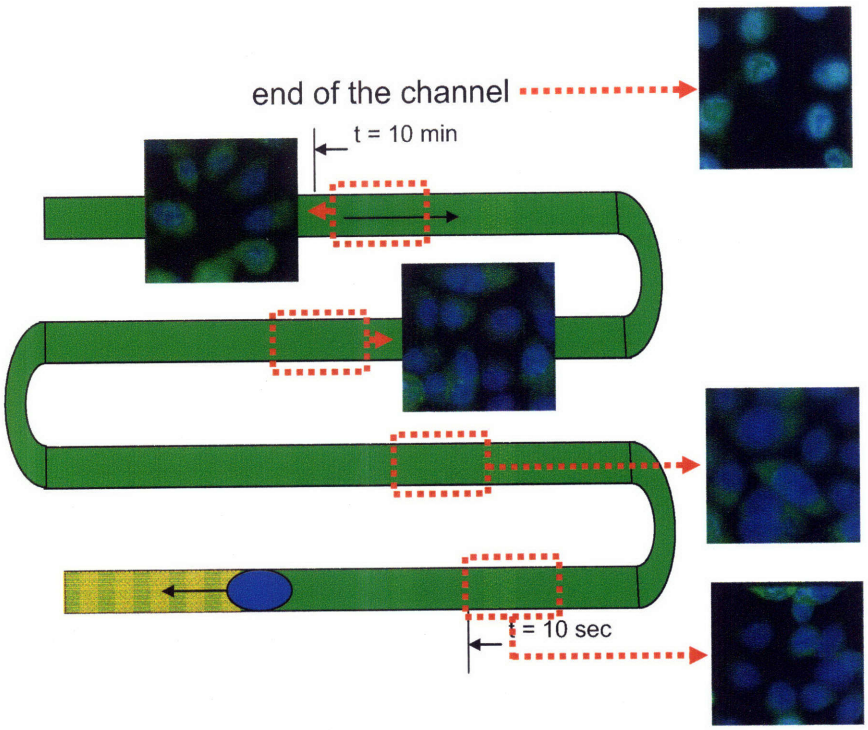

Figure 4.2. Fluorescence Imaging of HeLa Cells. The blue color in the images is DNA dye, and the green color is the fluorescence labeled with specific proteins. Notice the cells close to the bubble, which have short stimulation time, have relatively lower green fluorescence intensity compared the cells relatively far from the bubble, but the cells close to the end of the channel, which have long stimulation time, have much lower green fluorescence intensity.

4.2.2 Microfluidic Device Fabrication and Assembly

The microfluidic devices were the same as those described in Chapter 2, expect for being bound with a thin coverslip, not a glass slide.

4.2.3 Microscope Setup

In this thesis, a state-of-the-art Delta Vision microscope (Applied Precision, LLC, Issaquah, Washington) was used for the fluorescence measurement, which allows high resolution 3-dimensional restoration microscopy (Figure 4.3). The Delta Vision uses wide-field epifluorescence and a high precision robotic stage to take Z-sections through the speciment. A sophisticated deconvolution algorithm is then used to restore the out-of-focus blur that inevitably arises in such microscopy. The algorithm is restorative rather than subtractive, which means that all the fluorescence emitted from the specimen is used in to produce the final image. This optimizes the use of the excitation light resulting in minimal phototoxicity and photobleaching compared to alternative forms of microscopy such as confocal methods. The overall result of the deconvolution is the resolution that actually exceeds the 180nm limit of light microscopy. Another reason why this type of microscope was chosen is that it has a long travel stage (25 mm X by 50 mm Y). With this stage, the whole channel can be detected without changing the setup.

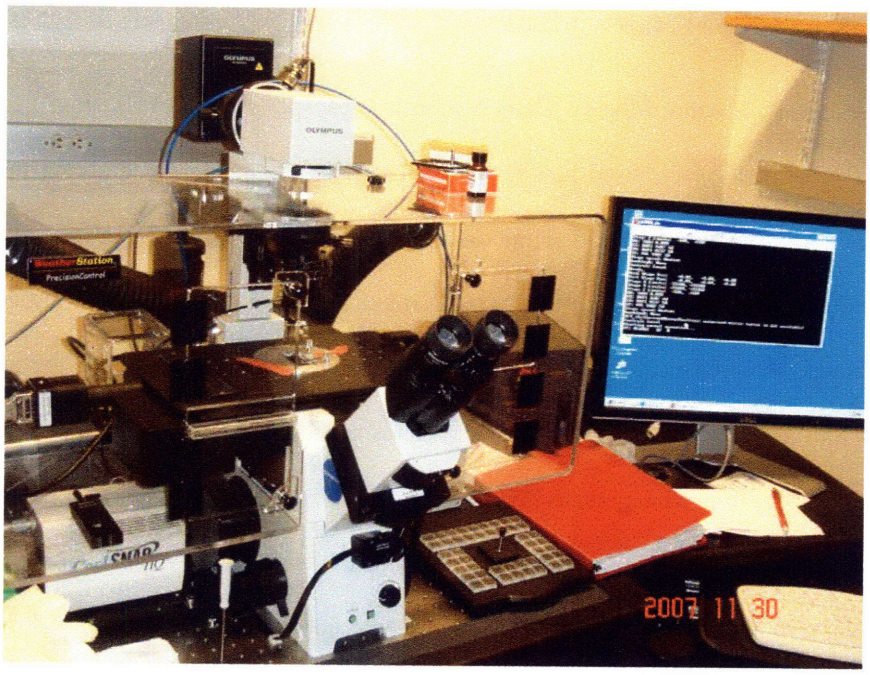

Figure 4.3. Delta Vision microscope. The hood around the microscope allows a constant incubation temperature for the growth of cells during the real-time imaging.

One of the issues was how to mount the microdevice in the microscope stage holder. The standard holder is a round steel plate with a 10 mm diameter observation hole in the center. This visible detection region is too small to measure the whole microchannels. A new design was required. Two holders were designed and machined. One of them (Figure 4.4) used a hold to fix the device between a plastic and steel plate. The advantage of this design was a large visible region and a flexible device shape. However, it has several disadvantages. First, the device was not held sufficiently stable and would move on the steel plate when the microscope stage was moving. Thus it was not able to

provide the precise location of the channels, and correspondingly, the time points associated with the cells in these positions were not accurate. Second, there was a large distance between the bottom of the microdevice and the bottom of the steel plate, which reduced the accessibility of the microscope objective detection region. Third, the microdevice was more easily broken by the hold; therefore, the second holder was designed (Figure 4.5). It was an aluminum holder to fit the stage of the microscope, engaging the three pins that support the disk to prevent the rotation of the holder when in place. The following lists describes the functions of each piece of the holder.

- Metal clips press a glass microscope slide against the top of the microdevice to eliminate curvature of surface.

- A minimally thick (.015") "ledge" for the device to rest on allows maximum access of the objective without collisions.

- The rectangular opening through the bottom of the insert aligns with the pattern on the device.

- The rectangular opening through the bottom of the holder is considerably smaller than the cell in order to provide maximum support for the thin coverslip on the bottom of the device, and to provide a firm counter for the force of the spring clips.

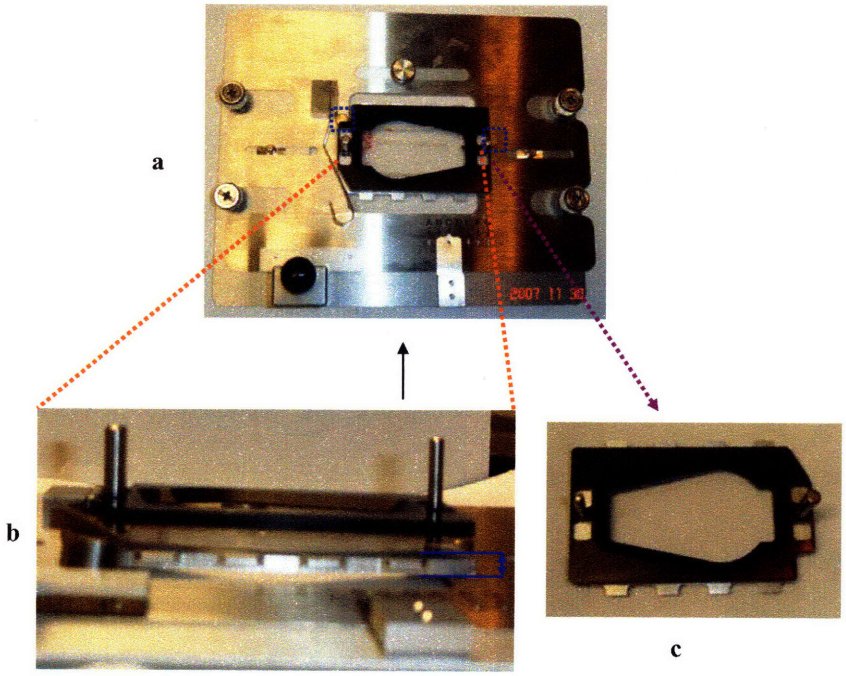

Figure 4.4. One of the microscope stage holders. a. a device hold set on a steel stage fix plate. The two poles marked with the blue dotted square is for fixing the two sides of the hold onto the steel plate. b. the front side view of the device held on the plate. c. the enlarged device hold.

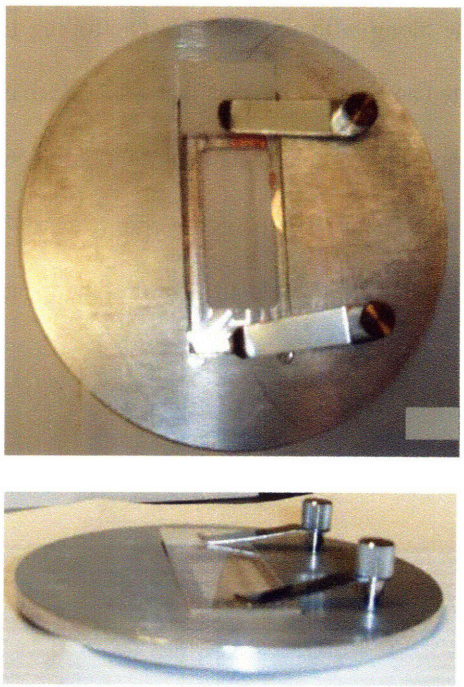

Figure 4.5. One microscope stage holder.

4.2.4 Analytical Methods

Analysis of p-ERK, p-JNK, and p-AKT signaling was done by using an immunocytochemical assay (In-Cell Western), as described in Chapter 3, except for a different second antibody and a DNA dye. The different second antibody Goat Anti-Mouse IgG 488 (1:200) (Invitrogen Corporation, Carlsbad, CA) was added with an additional one hour of incubation. After washing with PBS-T for another three times, a DNA dye DAPI (1:250) (Invitrogen Corporation, Carlsbad, CA) was injected into the channel and incubated for 20 min. The fluorescence was measured along the length of the channel by Delta Vision Deconvolution microscope.

The Delta Vision came along with the software controlling the movement of the microscope stage. We created an Excel worksheet that was used to calculate the points to be visited on the microchannel chip. The calculations were based on the measurement of the stage coordinates of two reference points on the chip (Figure 4.6) and interpolating the other points to be visited on the channels. In this way, the locations of cells at these points were accurately positioned.

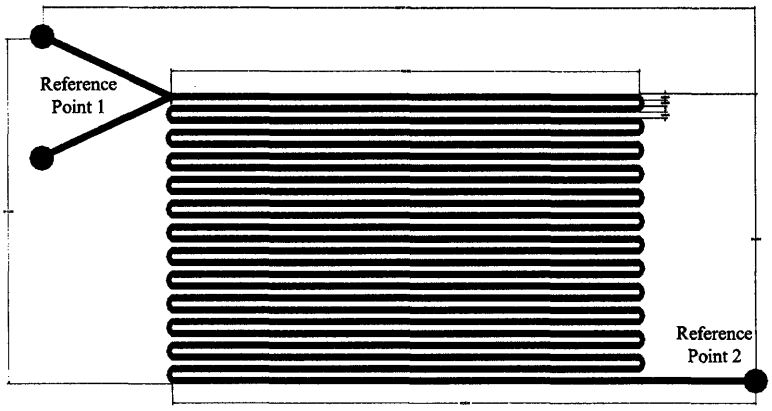

Figure 4.6. Located time positions in the microchannel.

Data analyzed based on the images were expressed as mean ± STD. Statistical analysis was performed by t test and F test.

4.2.5 Automatic Cell Signaling Counting

Cell signaling analysis is usually carried out by visual inspection of the image or manual counting. This procedure is time-consuming and not very objective. Therefore, an automatic cell signal counting method was introduced for accurate, fast and automatic

analysis. There are a number of benefits that result from an automated analysis: an acceleration of time and a reduction in cost for image analysis as well as a decrement in a false inspection due to fatigue. Additionally, the automated analysis provides a quantitative description of each particular cell in the image. Based on this quantitative measurement, the analysis result is objective. The quantitative description can be used as a concise representation of the image for efficient storage and quick retrieval.

A typical image of attached cells has the following characteristics that form the basis of our algorithm: 1) noise and artifacts; 2) various cell shapes and cell intensity overlapping; 3) inner points within a cell with a lower intensity; and 4) cell object sticking together. Several image segmentation techniques were investigated such as, contour-based, region-based and mixed contour-region-based methods [121], histogram-based and minimum-error-threshold [122], and watershed algorithm [121]. For cell imaging, none of the above methods could be used directly, so we developed the following algorithm to segment the cell images and count the cell objects. An automation of image analysis that previously required manual operations was performed on the basis of the developments in computer capabilities and image processing algorithms. [123-126]

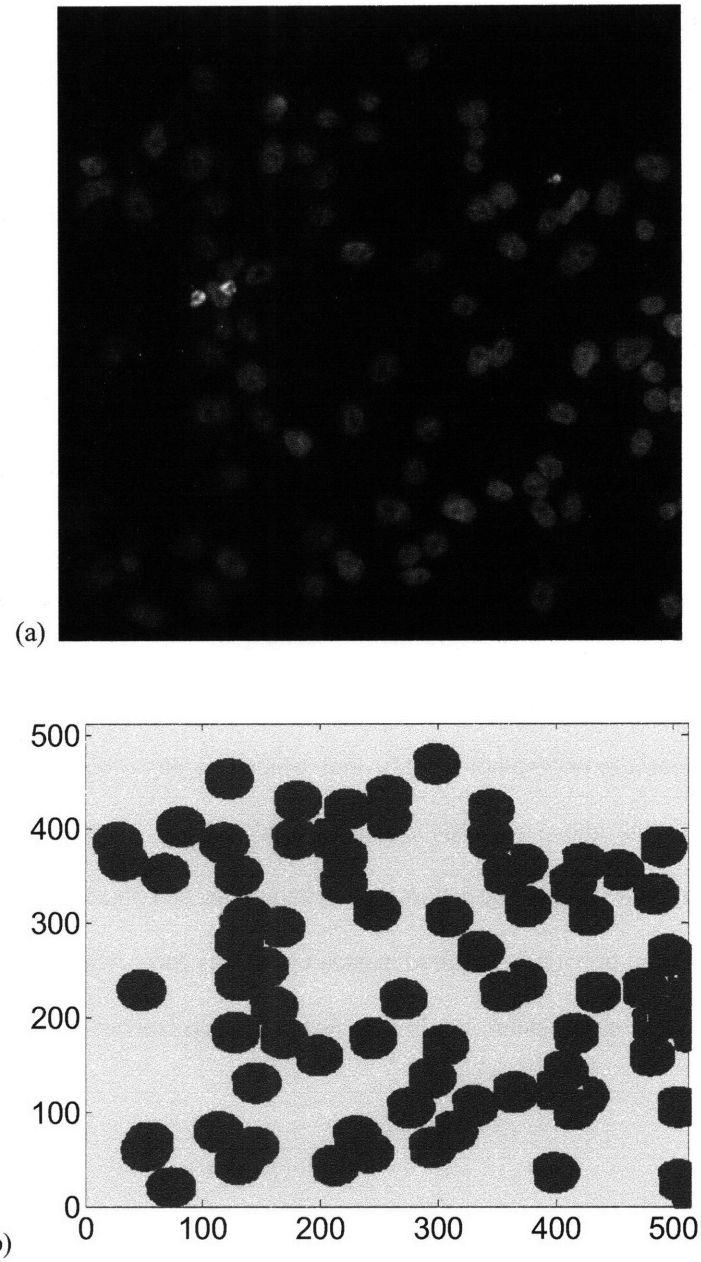

Figure 4.7. a. A typical microscopic image; b. The same image after cluster and morphology operations.

In this algorithm, the cell cluster detection was accomplished by comparing the size of the segmented regions to a preset size. If the region size was below the preset value, the region was considered an artifact; otherwise, the region was considered either a single cell or a cluster. Then, the distinction between the two was made based on another preset size value. If the size of the region was larger than an acceptable cell size, the region was then considered a cluster. The number of cells in a cluster was approximated by a simple division between the size of the region and a preset cell size. This detection algorithm was improved by searching the cell nuclear center with the first marker, and using this center to classify the cell signal cluster with the second marker. Figure 4.7.a shows a typical microscopic image. Figure 4.7.b shows the same image after cluster and morphology operations. This detection algorithm performed poorly when cell sizes varied extensively. Fortunately, cell size variations were moderate for the HeLa cells and HT29 cells used in these investigations.

4.3 Results and Discussion

4.3.1 Automatic Cell Counting

To verify the accuracy of the automatic counting, multiple experiments were performed and the resulting cell counting for each experiment was compared to a careful manual counting. Comparisons of four sample images of two cell lines are presented in Table 4-1.

Table 4-1. The results from sample images of HeLa cells and HT29 cells

Image		Manual Count	Auto Count	Error
HeLa Cells	1	131	134	2.3 %
	2	81	87	7.4 %
	3	77	75	-2.6 %
	4	82	80	-2.4 %
HT29 Cells	1	156	150	-3.8 %
	2	280	292	4.1 %
	3	120	122	1.6 %
	4	223	213	-4.5%

On average, the manual method took 3-4 minutes to count the cells in one image, and took 1 hour to manipulate and measure the fluorescence intensity of cells in one image, while the algorithms took approximately 30 second – 1 minute to count and measure the cells. Comparing, the cell counting results from the automatic method were very close to those determined manually (error within ± 11 %).

The image quality was affected by many factors. The exposure time, the filter, phase contrast, and frequency could affect the final cell image quality and thus affect the accuracy of this method. To refine the final result, mathematical morphology can be used

to further enhance the accuracy. In addition, by using fuzzy logic instead of a crisp threshold in the determination of the gradient, the result could perhaps become even more accurate.

4.3.2 Cytokine Signaling of HeLa and HT29 Cells Measured in the Microfluidic Device Based on Single Cells

p- ERK and p-JNK signaling of HeLa cells and HT29 cells were studied. In Figure 4.8 and Figure 4.9, the black dots represent the mean of the fluorescence intensity of the corresponding signal of all the single cells in one image. The variance bar expresses the standard deviation of the fluorescence intensity of single cells in this image. The blue diamonds represent the average fluorescence intensity of the cell signal based on cell population analysis, completed by the method described in Chapter 3. There is a significant difference in the variance, but no apparent correlation with the cell locations in the channels (stimulation time). The average cell signaling profiles based on single cell analysis and cell population analysis are comparable. Thus, the cell signaling from a small number of cells (~ 100-200) might be considered as the representation of that from a large number of cells (thousands). The important result is that Microfluidic method provided a useful technique for measuring the cell-to-cell variations while also tracking the average.

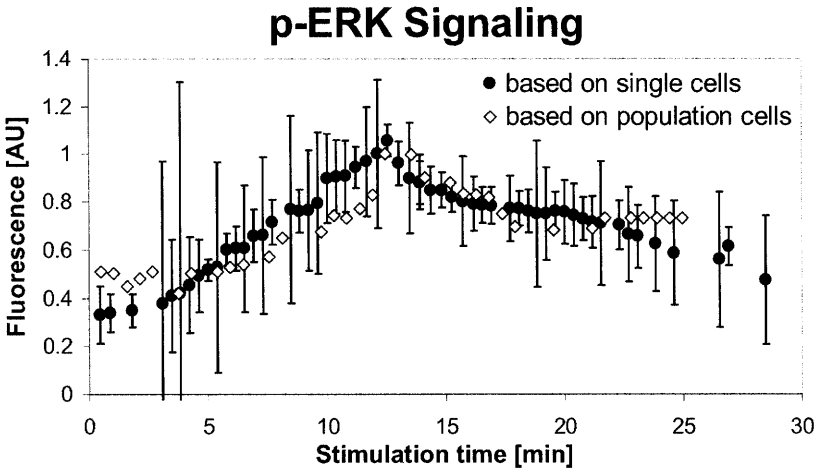

a.

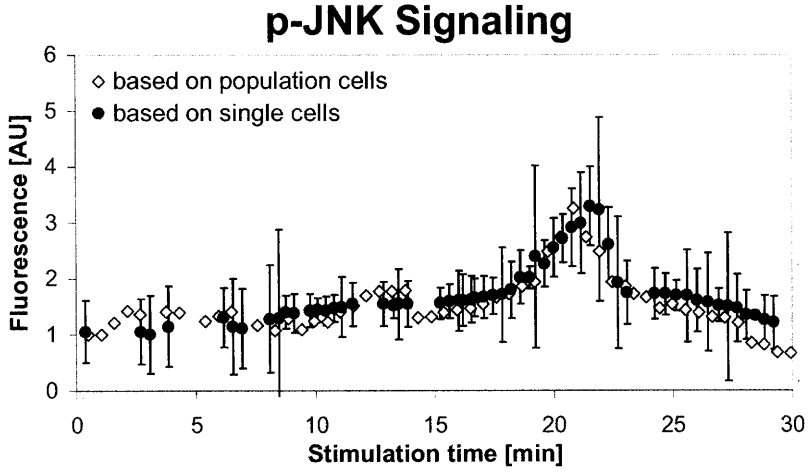

b.

Figure 4.8. a. p-ERK signaling of HeLa cells treated with EGF b. p-JNK signaling of HeLa cells treated with TNFα.

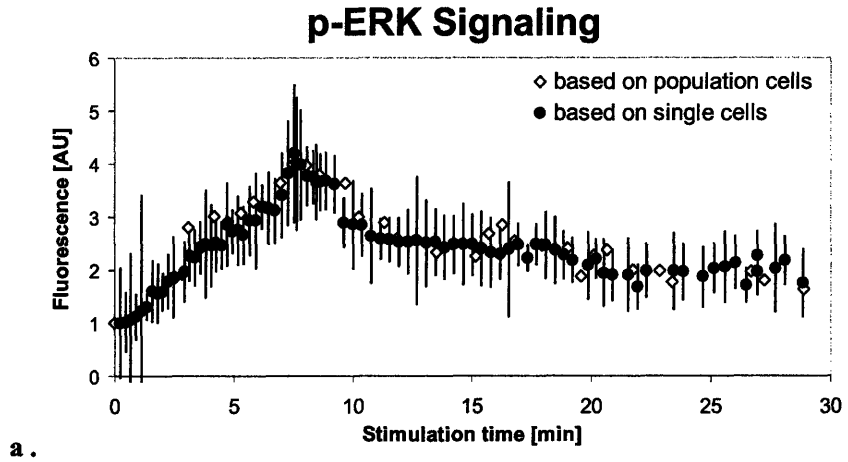

a.

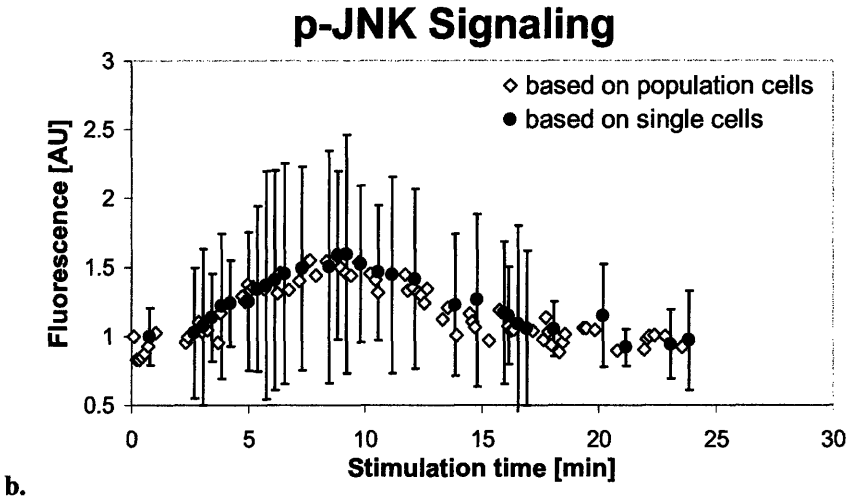

b.

Figure 4.9. a. p-ERK signaling of HT29 cells treated with EGF b. p-JNK signaling of HT29 cells treated with TNF.

In order to explore if the observed cell variance in response could be caused by the fluid in the microdevice, a statistical analysis was done on the experimental data.

Because of the parabolic flow profile of the laminar flow in the microchanel, the cells on the edge and in the center of the channels were exposed at different fluidic conditions. Therefore, two samples (cells on the edge and cells in the center) were compared by 2 tailed t test and F test. Two specific examples of HeLa cells and HT29 cells (Figure 4.10 and Figure 4.11), one with a relatively large cell variance, and the other with a small one, show that at 95% confidence, there is no significant difference between the two samples. All the other cases also showed the same results. Therefore, it could be said that the observed cell-to-cell variations are not caused by different fluid conditions in the microchannels.

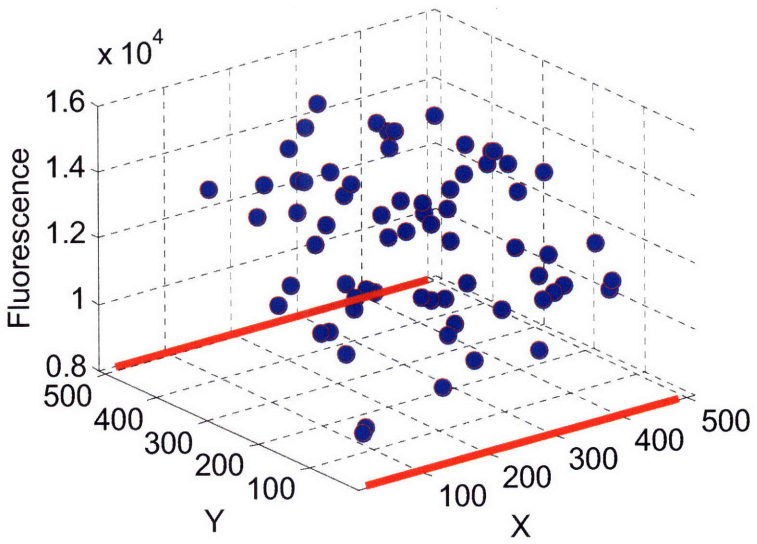

(a)

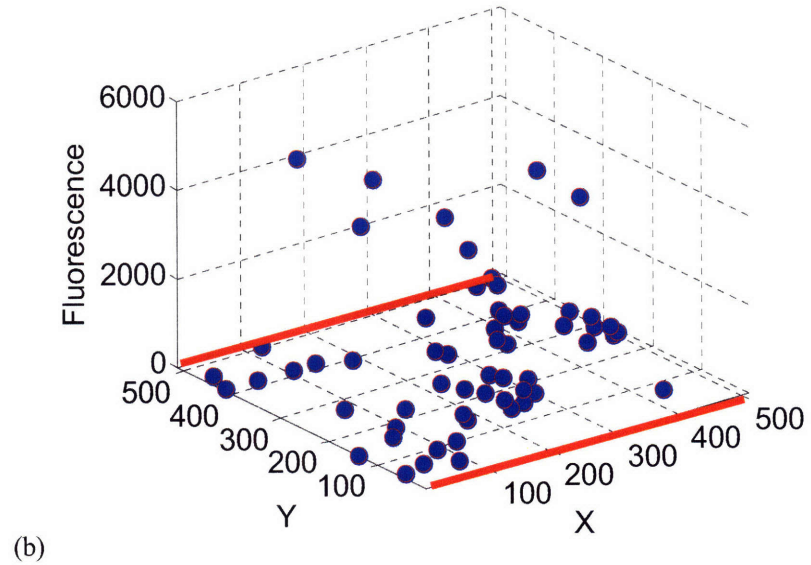

(b)

Figure 4.10. p-ERK signaling (a) and p-JNK signaling (b) of HeLa cells at different location. Notice x-y axis represents the position of cells and two red bold lines represent the walls of the microchannel.

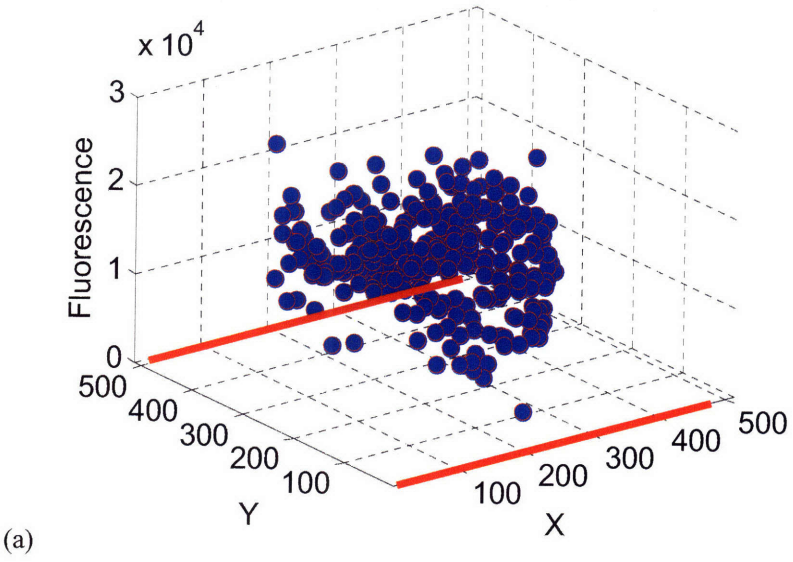

(a)

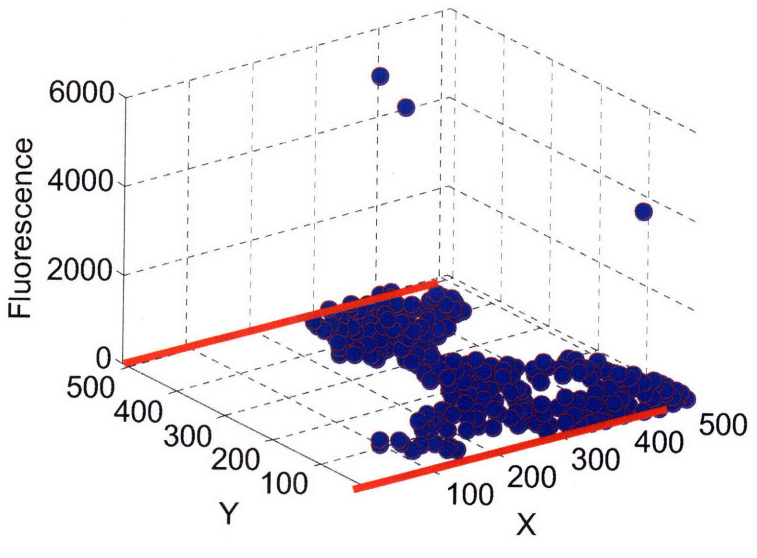

(b)

Figure 4.11. p-ERK signaling (a) and p-JNK signaling (b) of HT29 cells at different location Notice x-y axis represents the position of cells and two red bold lines represent the walls of the microchannel.

The fluctuations which underlie cell-to-cell variability can be separated into intrinsic and extrinsic ones [127,128]. Intrinsic fluctuations are those which result from a random occurrence of a defined set of reactions at random times, leading to cell-to-cell variability for genetically identical cells in identical and fixed environments. Extrinsic fluctuations can have multiple origins, such as fluctuations in cytoplasmic and nuclear volumes, in the initial state of the cell, signaling cascade fluctuations, or variations in the number of regulatory molecules. These cell-to-cell variations could be attributed to pre-existing differences in the cell-cycle position of individual cells at the time of pathway induction [127]. Another large component of the variation in system output could be cell-to-cell differences in the capacity of cells to express proteins. [130] Genetically identical cells had different protein expression, perhaps due to differences in the numbers of ribosomes or RNA polymerase II complexes, or the cellular energy level.

4.4 Conclusion

A microfluidic technique was developed for single-cell detection and analysis. A new microscope stage holder was designed and machined, and an automatic cell counting algorithm was developed for the single-cell analysis. The single-cell analysis provided significant cell-to-cell variations with stimulation times, along with the same average cell-signaling profiles as those based on the cell population analysis. Thus the integration of the single-cell imaging and microfluidic method proves to be a useful technique for exploring the cell signaling with single-cell resolution.

We hope that the combination of physiological experimentation done in the microfluidic devices enabled by new measurement tools and existing molecular and genetic methods will allow us to gain greater insight into the mechanisms that regulate quantitative variations. Understanding mechanisms that regulate the global capability to express proteins from genes might have applicability to protein expressions and the engineering of biological systems. Understanding the mechanisms that constrain variations in cell-fate decision systems might also enable new therapeutic interventions, for example to narrow the distributions of cellular responses to a pro-apoptotic anti-cancer drug.

Chapter 5. Conclusions and Recommendations for Future Opportunities

5.1 Principal Thesis Contributions

This thesis has explored the use of microfabrication technique in facilitating biological research. A number of "unit operations" for micro-scale cellular manipulation and analysis, including cell culture, cell stimulation, and protein analysis, have been combined in an effort to establish platforms for multi-functional and quantitative manipulations of the biological system. This thesis work resulted in disposable microdevices for replacing the time-consuming microwells and the manual western blotting with a single microfluidic device exploring the duality of space and time aligned with In-Cell Western.

This thesis has demonstrated the feasibility of culturing mammalian cells in microliter volumes up to one week in a batch reactor. A microdevice designed to provide sufficient oxygen to a growing culture was fabricated out of PDMS and glass. The technique developed provided a superior and viable alternative to the conventional cell culture in Petri dish or wells. Besides the cell culture, the cell growth was combined with the cell biochemical stimulation and the downstream protein analysis in a single microchip.

This thesis is the first to demonstrate the use of microfluidic devices for studying the protein pathways of adherent cells under a short stimulation time. A single microfluidic experiment produced a complete temporal response curve, which would have required multiple experiments and manual immunocytochemical assays by standard 96 wells and pipetting techniques. Stimulation of cells performed in the device resulted in pathway activation comparable to those from the conventional methods, and the good time control in the device resulted in reproducible analysis of fast transient responses in the cell signaling pathways.

This thesis is the first to explore the characterization of interactions between cells and the small extracellular flow. Mass transport and ligand binding reaction, along with the shear stress inducing cell responses, were investigated and used for explaining the cell signaling phenomena. Shear stress is the tangential component of hemodynamic forces acting on the vessel wall and constitutes a risk factor of cardiovascular diseases. It is important and valuable to study the shear stress effect. This thesis provides a microfluidic technique for potential studies of the kinetics of cell signaling triggered by the bound ligands, which could be not be accomplished by the conventional technique.

Lastly, this thesis has demonstrated the use of microfluidic technique for single-cell detection and analysis. A new microscope stage holder was designed and machined, and an automatic cell counting algorithm was developed for the single-cell analysis. The single-cell analysis provided the cell variations and the mean with the stimulation time. It gave the same average cell signaling profiles as those based on the cell population

analysis. It further indicated that it may be feasible to use a small number of cells to predict population cell events. This technique also provided useful insight into the cell variation and the cell signaling. It also provides quantitative information about the local and temporal heterogeneities in the behavior of cells with statistical distributions. This advantage of single-cell measurements is effectively applicable to the quantitative analysis of cell signaling processes that are unavoidably affected by the local heterogeneity of cell-cycle positions. Using single-cell imaging, we will have, to our knowledge, for the first time to observe and quantify the amplification mechanism of cell signaling induced by dynamic clustering of receptors. We believe that the applications of these devices could be helpful in future fundamental studies of the cell signaling for biotechnology and therapeutic applications.

5.2 Future Opportunities

5.2.1 Materials and Surfaces

PDMS was used as the primary material of construction for the microfludic device fabricated in this thesis. Biocompatibility, transparency, and rapid prototyping of designs using standard soft lithographic techniques were the primary motivations for using this material. However, high temperature during autoclaving can cause it to be deformed, especially when it was bounded with a very thin glass slide. This deformation made auto-scanning under the microscope difficult, resulting in the objective having to be manually adjusted to obtain a good focus, a time-consuming and laborious procedure. PDMS is, therefore, not the final appropriate material of construction envisioned for the

devices in future applications. Several other materials, such as glass or polymers, could be used for the fabrication of the microchannels.

A thermal stage and incubator were used to maintain the experimental temperature and cell culture environment. For future applications, portable, self-contained, maintenance-free, and long-term cell culture systems are desirable. The complex gas supply, optical and heating systems are needed to eliminate the need for an incubator or an external CO_2 source to maintain cell culture and preclude the need for chip removal/realignment to perform optical observations. PDMS membrane valves could be used for CO_2 supply. A transparent controlled heater may be attached to the device and used for heating. To implement a heated observation area, a slide glass with a flexible transparent heater can be attached flush to the fingerplate. The cultivation area can be in full contact with the surface of the slide glass and be heated through the slide glass. Heating the PDMS chip through the glass slide can make the temperature more uniform at the PDMS surface compared to applying the transparent heater directly to the chip. Temperature can be controlled by a digital temperature controller and a thermocouple integrated on the surface of the slide glass. This system will allow the culture of highly CO_2-dependent cells continuously in a non-37 °C, non-CO_2-rich, non-humidified and non-sterile atmosphere with real-time cell imaging.

5.2.2 Microfluidic devices for future Biology studies

This thesis has explored examples of micro-bioanalysis, and has initiated additional opportunities for the use of microdevices in biological research. Possible future work

includes new applications of these devices for the study of other interesting cell signaling pathways (as shown in Figure 5.1), the optimization, automation, and further generalization of these devices, and the integration of unit operations. However, the availability of the antibodies for In-Cell Western is a challenge. These integrated devices could potentially automate all the unit operations for biological research, as shown in Figure 5.2.

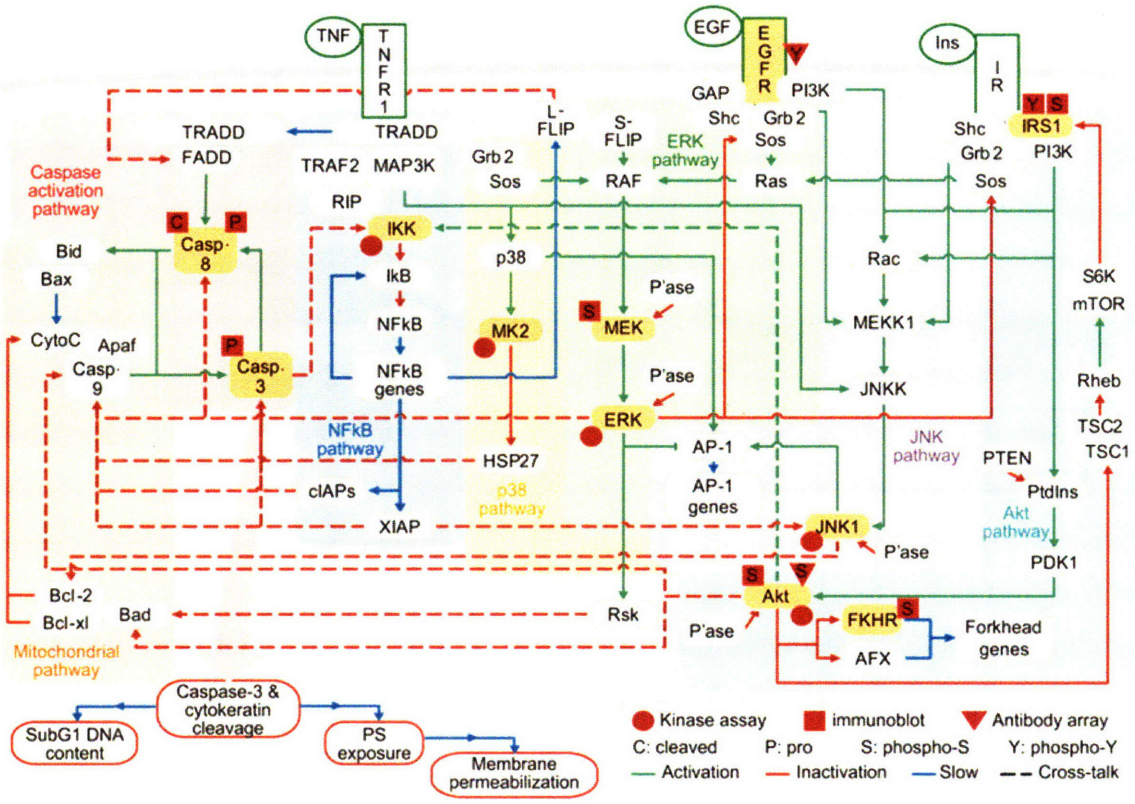

Figure 5.1. Cell signaling pathways

Breakthroughs in microfluidic technology are rapidly bringing the long-awaited potential of microfluidics to fruition. The recent acceleration of progress in this field has

allowed levels of complexity and functionality to be routinely achieved on chip. However, the obstacles to the integration are not trivial. But the integration and judicious application of these tools to important biological problems that can benefit both from the economy of the scale and from the physical properties that are manifested on the micrometer length scale will ensure that the full impact of these advances is felt in the near future. Microfluidic devices will enable many new innovative tools in system and structural biology for the optimization of growth conditions, on-chip protein purification and solubility detection, and DNA and RNA separation and detection.

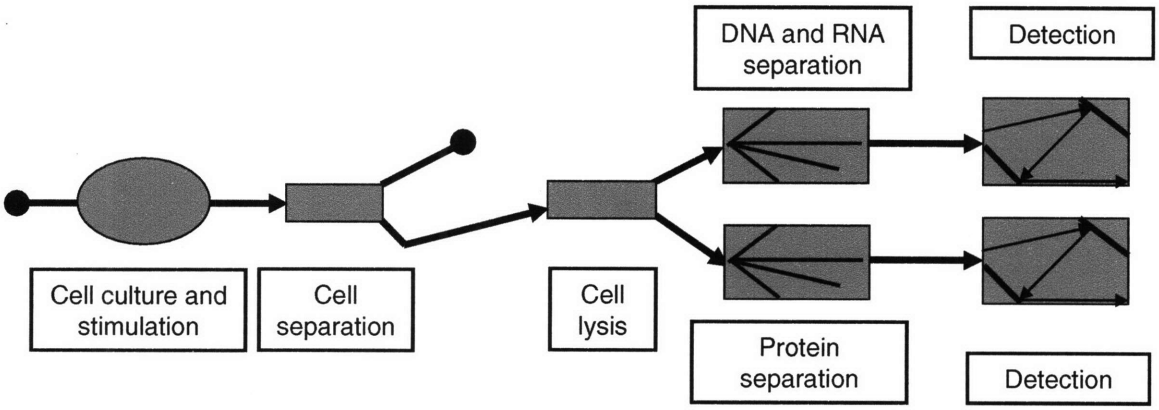

Figure 5.2. Integrated, multifunctional, and chip-based device for biological and biochemical analysis.

Appendix A: Process Sequence for SU-8 masters

The process to fabricate a SU-8 master follows KFJ group recipe. The equipment names in the parentheses refer to machines in the Technology Research Laboratory (TRL) in MIT's Microsystems Technology Laboratories (MTL). The starting substrate is a 4" Silicon wafer (SSP, Test grade). The entire process is code purple. A two layer coating process is used to ensure uniform layer thickness over the entire wafer.

Process Steps

1. Dehydration Bake: Bake the wafers on a hotplate at 200 °C for 20 min. This step removes any adsorbed moisture on the silicon wafer.

2. Spin coating of first SU-8(2050) layer: Transfer the wafers immediately from the dehydration bake hotplate to the spin coater (SU-8 spinner/ TRL) using a metallic wafer carrier. The wafer cools rapidly when placed on the metallic spin coater chuck. Use a nitrogen gun to blow away any dust particles on the wafer. Dispense a small amount (~20 mm diameter circle) of SU-8(2050) (Microchem Corp., MA) onto the wafer and start spinning immediately. SU-8(2050) has a quick evaporating solvent base, therefore immediate spinning is necessary. Spin at 650 rpm for 15s and 1100 rpm for 35s. This yields a layer of thickness ~100-150 μm.

3. Soft-bake of first SU-8(2050) layer: Transfer the freshly coated wafer to a hot plate. Heat at 65 °C for 10 minutes, ramp up to 95 °C and hold for 45 minutes. Cool to at least 65 °C before transferring to the spin coater for the next step.

4. Spin coating of second SU-8(2050) layer: Same sequence of steps as 2.

5. Soft-bake of second SU-8(2050) layer: Same sequence of steps as 3.

6. Photolithography to define microchannel pattern: Interval exposure (5s x 17, 4s interval) (EV1/TRL).

7. Post-exposure bake: Place the freshly exposed wafer to a hot plate. Heat at 65 °C for 10 minutes, ramp up to 95 °C and hold for 30 minutes. Cool to at least 50 °C before transferring for development.

8. Development: Develop in poly(glycol)mono ether acetate (PGMEA,

Microchem.) for 45 min, replace with fresh solution every 15 min.

9. Washing: Rinse with Isopropyl alcohol and dry under a stream of nitrogen.

Appendix B: Dimension of the Microscope Stage Insert

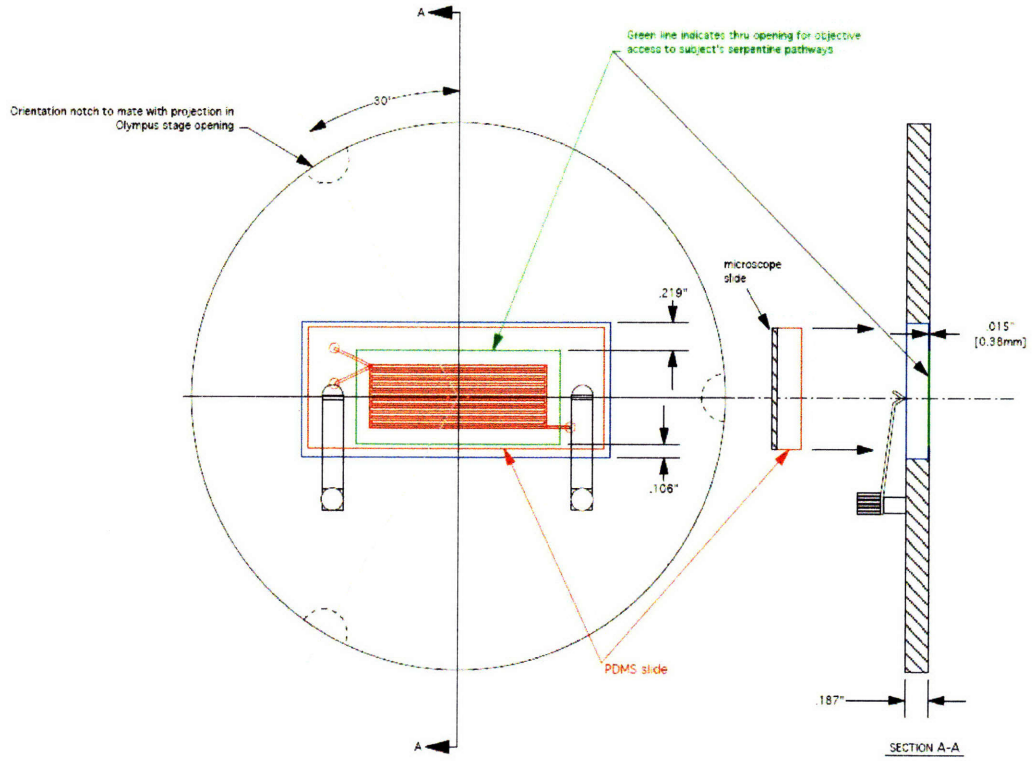

Appendix C: Matlab Code for Auto Cell Signal Analysis

```
function cell_count()
close all;
clear all;
N=3;
fid=fopen('result.txt','w');
for n=3:N
    filename1=sprintf('%d_w457.tif',n);
    filename2=sprintf('%d_w528.tif',n);
    process_pic_2(filename1,filename2,fid)
end
fclose(fid);

function process_pic_3(filename1,filename2,fid)

threshold_nucleus=10000;

threshold_distance=15;
center=[];
collection=[];
current=[];
n_class=0;
A = imread(filename1,'TIF');
[m,n]=size(A);
% Find cell center by nucleus pic
for i=1:m
    for j=1:n
        if A(i,j)>threshold_nucleus
            belong=0;
            % creat first class
            if n_class==0
                n_class=n_class+1;
                center(1,:)=[i j];
                collection(1,1)=i;
                collection(1,2)=j;
                current(1)=1;
                belong=1;
            else
                % add to one existed class
                for k=1:n_class
                    if norm(([i j]-center(k,:)))<threshold_distance
                        current(k)=current(k)+1;
                        collection(current(k),2*k-1)=i;
                        collection(current(k),2*k)=j;
                        center(k,1)=mean(collection(1:current(k),2*k-
1));
                        center(k,2)=mean(collection(1:current(k),2*k));
```

```
                        belong=1;
                        break;
                    end
                end
                % creat a new class if it does not belong any class
                if belong==0
                    n_class=n_class+1;
                    center(n_class,:)=[i j];
                    current(n_class)=1;
                    collection(1,2*n_class-1)=i;
                    collection(1,2*n_class)=j;
                    belong=1;
                end
            end
            %B(i,j)=1;
        else
            %B(i,j)=0;
        end
    end
end

% Compute average intensity for each cell and whole average and
standard
% deviation by cell pic

threshold_cell=3000;
threshold_distance=20;
num_cell=size(center,1);
collection=[];
current=zeros(num_cell,1);
A = imread(filename2,'TIF');
[m,n]=size(A);

for i=1:m
    for j=1:n
        if A(i,j)>threshold_cell
            for k=1:n_class
                if norm(([i j]-center(k,:)))<threshold_distance
                    current(k)=current(k)+1;
                    collection(current(k),2*k-1)=i;
                    collection(current(k),2*k)=j;
                    break;
                end
            end
            B(i,j)=1;
        else
            B(i,j)=0;
        end
    end
end

ave_inten=zeros(n_class,1);
```

```
for i=1:n_class
    for j=1:current(i)
        ave_inten(i)=((j-1)*ave_inten(i)+double(A(collection(j,2*i-
1),collection(j,2*i))))/j;
    end
end

center, ave_inten
cellA=[];
cellB=[];
numA=0;
numB=0;
for j=1:n_class
    celledge=512-20;
    if center(j,1)>=celledge / center(j,2)>=celledge / center(j,1)<=20
/ center(j,2)<=20
        numA=numA+1;
        cellA(numA)=ave_inten(j);
    else
        numB=numB+1;
        cellB(numB)=ave_inten(j);
    end
end
st_A=std(cellA(1:numA))
numA
st_B=std(cellB(1:numB))
numB
st_AB=std(ave_inten);
n_class

%ave_inten
whole_ave=mean(ave_inten);
whole_std=std(ave_inten);
fprintf(fid,'%d %f %f ',n_class,whole_ave,whole_std);
fprintf(fid,'%f ',ave_inten);
fprintf(fid,'\n');
x=center(:,1);
y=center(:,2);
z=ave_inten;
figure(1)
plot3(x,y,z,'ro');
%figure(2)
%N=hist(z);
% for n=1:n_class
% plot(collection(n:current(n),2*n-
1),collection(n:current(n),2*n),'*');
% hold on
% end
% hold off
% figure;
% colormap(gray);
```

```
% imagesc(B)
% figure;
% colormap(gray);
% imagesc(A)
```

Reference

1. Schlessinger J. Cell signaling by receptor tyrosine kinases. Cell 2000; 103:211–225.

2. De Meyts P, Whittaker J. Structural biology of insulin and IGF1 receptors: implications for drug design. Nat Rev Drug Discov 2002; 1:769–783.

3. Wolf B, Kraus M, Brischwein M, Ehret R, Baumann W, Lehmann M. Biofunctional hybrid structures-cell-silicon hybrids for applications in biomedicine and bioinformatics. Bioelectrochem Bioenerg 1998;46:215–225.

4. Kevin Janes, Suzanne Gaudet, John G. Albeck. Cell. 2006; 124: 1225–1239.

5. Pawson T, Nash P. Assembly of cell regulatory systems through protein interaction domains. Science 2003; 300:445–452.

6. Dufner, A., and Thomas, G.. Exp Cell Res 1999;253:100-109.

7. Voldman J, Gray ML, Schmidt MA. Microfabrication in biology and medicine.Ann Rev Biomed Eng 1999;1:401– 425.

8. Paegel BM, Blazej RG, Mathies RA. Microfluidic devices for DNA sequencing: sample preparation and electrophoretic analysis. Curr Opin Biotechnol 2003;14:42–50.

9. Mastrangelo CH, Burns MA, Burke DT. Microfabricated devices for genetic diagnostics. Proc IEEE 1998;86:1769 –1787.

10. Beebe DJ, Mensing GA, Walker GM. Physics and applications of microfluidics in biology. Annu Rev Biomed Eng 2002;4:261–286.

11. Lahann J, Balcells M, Lu H, Rodon T, Jensen KF, Langer R. Reactive polymer coatings: a first step toward surface engineering of microfluidic devices. Anal Chem 2003;75:2117–2122.

12. Fritz J, Baller MK, Lang HP, Rothuizen H, Vettiger P, Meyer E, Gu¨ ntherodt H-J, Gerber C, Gimzewski JK. Translating biomolecular recognition into nanomechanics. Science 2000;288:316–318.

13. Han J, Craighead HG. Separation of long DNA molecules in a microfabricated entropic trap array. Science 2000;288:1026– 029.

14. Jamil El-Ali, Peter Sorger, and Klavs F. Jensen. Nature. 2006; 442:403-411.

15. Kholodenko, B. N.; Demin, O. V.; Moehren, G.; Hoek, J. B. J. Biol. Chem. 1999; 274:30169-30181.

16. Hudson TJ, Stein LD, Gerety SS, Ma J, Castle AB, et al. An STS-based map of the human genome. Science 1995;270:1945–1954.

17. Chervitz SA, Aravind L, Sherlock G, all CA, Koonin EV, et al. Comparison of the complete protein sets of worm and yeast: orthology and divergence. Science 1998;282:2022–2028.

18. Adams MD, Celniker SE, Holt RA, Evans CA, Gocayne JD, et al. The genome sequence of Drosophila melanogaster. Science 2001;287:2185–2195.

19. Fodor SP, Read JL, Pirrung MC, Stryer L, Lu AT, Solas D. Light-directed, spatially addressable parallel chemical synthesis. Science 1991;251:767–773.

20. Lam KS, Salmon SE, Hersh EM, Hruby VJ, Kazmierski WM, Knapp RJ. A new type of synthetic peptide library for identifying ligand-binding activity. Nature 1991;354:82–84.

21. Hacia JC, Fan JB, Ryder O, Jin L, Edgemon K, et al. Determination of ancestral alleles for human single-nucleotide polymorphisms using high-density oligonucleotide arrays. Nat. Genet. 1999;22:164–167.

22. Gilles PN, Foster CB, Dillon PJ, Chanock SJ, Wu DJ. Single nucleotide polymorphic discrimination by an electronic dot blot assay on semiconductor microchips. Nat. Biotechnol.1999;17:365–370.

23. Xu X, Miller C, Wang L, Edman CF, NerenbergM, Westin L. Anchored multiplex amplification on a microelectronic chip array. Nat. Biotechnol. 2001;18:199–204.

24. Fernandez-Botran R, Chilton PM, Ma Y. Soluble cytokine receptors: their roles in immunoregulation, disease, and therapy. Adv Immunol 1996;63:269–336.

25. Orkin SH. Development of the hematopoietic system. Curr Opin Genet Dev 1996;6:597–602.

26. Bazan JF. Structural design and molecular evolution of a cytokine receptor superfamily. Proc Natl Acad Sci U S A 1990;87:6934–8.

27. Golstein P. Cell death: TRAIL and its receptors. Curr Biol 1997;7:R750–3.

28. Nagata S. Fas ligand-induced apoptosis. Annu Rev Genet 1999;33:29–55.

29. Cohen GM. Caspases: the executioners of apoptosis. Biochem J 1997;326:1–16.

30. Wajant H, Pfizenmaier K, Scheurich P. Tumor necrosis factor signaling. Cell Death Differ 2003;10:45–65.

31. Chen G, Goeddel DV. TNF-R1 signaling: a beautiful pathway. Science 2002;296:1634–5.

32. Fallon JH, Seroogy KB. et. al. Epidermal growth factor immunoreactive material in the central nervous system: location and development. Science 1984;224: 1107-1109.

33. W. X. Schulze, L. Deng and M. Mann. Phosphotyrosine interactome of the ErbB-receptor kinase family. Molecular systems biology 2005; 1.

34. N. Zarich, J. L. Oliva, N. Martinez, R. Jorge, A. Ballester, S. Gutierrez-Eisman, S. Garcia-Vargas and J. N. Rojas. Grb2 Is a Negative Modulator of the Intrinsic Ras-GEF Activity of hSos1. Molecular Biology of the Cell Epub ahead of print 2006.

35. J. Avruch, A. Khokhlatchev, J. M. Kyriakis, Z. Luo, G. Tzivion, D. Vavvas and X. F. Zhang. Ras activation of the Raf kinase: tyrosine kinase recruitment of the MAP kinase cascade. Recent Progress in Hormone Research 2001;56:127-155.

36. Carpenter G, and Cohen S. Epidermal growth factor. J. Biol. Chem. 1999;265:7709-7712.

37. Minuto F, Del Monte P, Barreca A, et al. Evidence for an increased somatomedin-C/insulin-like growth factor 1 content in primary human lung tumors. Cancer Res 1986;46:985–988.

38. Yee D, Paik S, Lebovic G, et al. Analysis of insulin-like growth factor I gene expression in malignancy: evidence for a paracrine role in human breast cancer. Mol Endo 1989;3:509–517.

39. Tricoli J, Rall L, Karakousis C, et al. Enhanced levels of insulinlike growth factor messenger RNA in human colon carcinomas and liposarcomas. Cancer Res 1986;46:6169–6173.

40. Zhan JM, Stampfer MJ, Giovannucci E, et al. Plasma insulinlike growth factor-I and prostate cancer risk: A prospective study. Science 1998;279:563–566.

41. Peyrat JP, Bonneterre J, Hecquet B, et al. Plasma insulin-like growth factor-1 (IGF-1) concentrations in human breast cancer. Eur J Cancer 1993;29A:492–497.

42. Turner BC, Haffty BG, Narayanan L, et al. Insulin-like growth factor-I receptor overexpression mediates cellular radioresistance and local breast cancer recurrence after lumpectomy and radiation. Cancer Res 1997;57:3079–3083.

43. Adams TE, Epa VC, Garrett TP, Ward CW. Structure and function of the type 1 insulin-like growth factor receptor. Cell Mol Life Sci 2000;57:1050–1093.

44. Grimberg A, Cohen P. Role of insulin-like growth factors and their binding proteins in growth control and carcinogenesis. J Cell Physiol 2000;183:1–9.

45. Petley, T., Graff, K., Jiang, W., Yang, H., and Florini, J.. Horm Metab Res 1999; 31:70- 76.

46. Rosenthal, S. M., and Cheng, Z. Q.. Proc Natl Acad Sci U S A 1995;92: 10307-10311.

47. Coolican, S. A., Samuel, D. S., Ewton, D. Z., McWade, F. J., and Florini, J. R. J Biol Chem 1997;272:6653-6662.

48. Marte, B. M., and Downward, J.. Trends Biochem Sci 1997;22:355-358.

49. Alessi, D. R., and Cohen, P.. Curr Opin Genet Dev 1998;8:55-62.

50. Leevers, S. J., Vanhaesebroeck, B., and Waterfield, M. D.. Curr Opin Cell Biol 1999;11:219-225.

51. T. H. Park and M. L. Shuler. Biotechnol. Prog., 2003;19:243–253.

52. G. M.Walker, H. C. Zeringue and D. J. Beebe. Lab Chip, 2004;4:91–97.

53. K. Viravaidya, A. Sin and M. L. Shuler. Biotechnol. Prog., 2004;20:316–323.

54. A. Sin, K. C. Chin,M. F. Jamil, J.Kostov, G. Rao and M. L. Shuler. Biotechnol. Prog., 2004;20:338–345.

55. I. K. Glasgow, H. C. Zeringue, D. J. Beebe, S.-J. Choi, J. T. Lyman, N. G. Chan and M. B. Wheeler. IEEE Trans Biomed Eng, 2001;48:5.

56. D. Beebe, M. Wheeler, H. Zeringue, E. Walters and S. Raty. Theriogenology, 2002;57:125–135.

57. E. M. Walters, S. G. Clark, D. J. Beebe and M. B. Wheeler, Methods. Mol. Biol., 2004;254:375–82.

58. S. Raty, E. Walters, J. Davis, H. Zeringue, D. Beebe, S. L. Rodriguez-Zas and M. B. Wheeler. Lab Chip, 2004;4:186–190.

59. G. M. Walker, M. S. Ozers and D. J. Beebe. Biomed. Microdevices, 2002;4:161–166.

60. S. Takayama, J. C. McDonald, E.Ostuni, M. N. Liang, P. J. A.Kenis, R. F. Ismagilov and G. M. Whitesides. Proc. Natl. Acad. Sci. USA,1999;96:5545.

61. B. S. Cho, T. G. Schuster, X. Zhu, D. Chang, G. D. Smith and S. Takayama. Anal. Chem., 2003;75:1671–1675.

62. S. Takayama, E. Ostuni, P. LeDuc, K. Naruse, D. E. Ingber and G. M. Whitesides. Nature, 2001;411:1016–1016.

63. S. Takayama, E. Ostuni, P. LeDuc, K. Naruse, D. E. Ingber and G. M. Whitesides. Chem. Biol, 2003;10:123–130.

64. A. Sawano, S. Takayama, M. Matsuda and A. Miyawaki. Dev. Cell, 2002;3:245–257.

65. H. Kaji, M. Nishizawa and T. Matsue. Lab Chip, 2003;3:208–211.

66. Paul J. Hung, Philip J. Lee, Poorya Sabounchi, Robert Lin and Luke P. Lee. Biotechnology and Bioengineering, 2005;89:1-8.

67. G. Banker and K. Golsin. The MIT Press, 1998:2nd ed.ch.13.

68. K. King, H. Terai, C. Wang, J.P. Vacanti, and J.T. Borenstein, Proc. MicroTAS2001, Monterey USA, 2001;247-249.

69. A. Rotem, M. Toner, R.G. Tompkins, and M.L. Yarmush, Biotechnol. Bioeng. 1992;40:1286-1291.

70. J.T. Borenstein, H. Terai, K. King, E.J. Weinberg, M.R. Kaazempur-Mofrad, and J.P. Vacanti, Biomed. Microdev. 2002;4: 167-175.

71. Moor, A. N.; Murtazina, R.; Fliegel, L. J. Mol. Cell. Cardiol. 2000;32:925-936.

72. Zhou, W.; Chen, C. C.; Buckland, B.; Aunins, Biotechnol. Bioeng. 1997;55:783 - 792.

73. Ozturk, S. S.; Palsson, O. Biotechnol. Bioeng. 1991;37:989-993.

74. Takagi, M.; Hayashi, H.; Yoshida, T. Cytotechnology 2000;32:171-179.

75. Lin, J.; Takagi, M.; Qu, Y.; Gao, P.; Yoshida, T. Cytotechnology 1999;29:27-33.

76. Lezama, R.; Diaz-Tellez, A.; Ramos-Mandujano, G.; Oropeza, L.; Pasantes-Morales, H. Neurochem. Res. 2005;30:1589-1597.

77. Wu, M. H.; Dimopoulos, G.; Mantalaris, A.; Varley, J. Biotechnol. Appl. Biochem. 2004;40:41-46.

78. Haab, B. B. Proteomics, 2003;3:2116–2122.

79. Speicher, M. R. & Carter, N. P. Nat. Rev. Genet., 2005;6:782–792.

80. Wheeler, D. B., Carpenter, A. E.&Sabatini, D. M. Nat. Genet., 2005;37:S25–S30.

81. J. Khandurina and A. Guttman, Curr. Opin. Chem. Biol., 2002;6:359–366.

82. V.C. Abraham, D.L. Taylor, and J.R. Haskins, Trends Biotechnol., 2004; 22:15–22.

83. A. Groisman, M. Enzelberger, and S.R. Quake, Science, 2003;300:955–958.

84. O. Worz, K.P. Jackel, T. Richter, and A. Wolf, Chem. Eng. Sci., 2001;56:1029–1033.

85. R.B. Bird, W.E. Stewart, and E.N. Lighttfoot, Transport Phenomena (John Wiley & Sons, 2002).

86. P.Watts and S.J. Haswell, Curr. Opin. Chem. Biol., 2003; 7:380–387.

87. J.C. McDonald and G.M. Whitesides, Acc. Chem. Res., 2002; 35:491–499.

88. P.J. Hung, P.J. Lee, P. Sabounchi, N. Aghdam, R. Lin, and L.P. Lee, Biotechnol. Bioeng., 2005; 89:1–8.

89. T.C. Merkel, V.I. Bondar, K. Nagai, B.D. Freeman, and I. Pinnau, J. Polym. Sci. B-Polym. Phys., 2000; 38:415–434.

90. J. Liu, C. Hansen, and S.R.Quake,Anal. Chem., 2003; 75:4718–4723.

91. I. Braslavsky, B. Hebert, E. Kartalov, and S.R. Quake, Proc. Nat. Acad. Sci. USA, 2003;100:3960–3964.

92. M.O. Reese, R.M. van Dam, A. Scherer, and S.R. Quake, Genome Res., 2003; 13:2348–2352.

93. Lauffenburger, D. A., and J. J. Linderman. Oxford University Press, New York. 1993.

94. Hendriks, B. S., L. K. Opresko, H. S. Wiley, and D. Lauffenburger. J. Biol. Chem. 2003; 278:23343–23351.

95. Michael I. Monine, Alexander M. Berezhkovsk, Elizabeth J. Joslin, H. Steven Wiley, Douglas A. Lauffenburger, and Stanislav Y. Shvartsman. Biophysical Journal. 2005; 88:2384–2390.

96. Gervais, T, and Jensen, K.F. Chem. Eng. Sci. 2006; 61:1102-1109.

97. B. S. Cho, T. G. Schuster, X. Zhu, D. Chang, G. D. Smith and S. Takayama. Anal. Chem., 2003; 75:1671–1675.

98. Li S, Kim M, Hu YL, Jalali S, Schlaepfer DD, Hunter T, Chien S, and Shyy JY. J. Biol. Chem. 1997; 272:30455-30462.

99. Yingxiao W, Joann C, Yi-chen L, Yi-shuan L, John S, and Shu C. J. Physiol Heart Circ Physiol. 2004; 286:H685-H692.

100. James S, Ryan J.H, Xinchun P, Masanori Y, Chen Y, and Bradford C.B. PNAS. 2001; 98:6476-6481.

101. Young-Mi G, Heonyong P, Matthew C.M, Victor M.D, Borislaw S, Reinhard W, and Hanjoong J. Am. J. Physiol. 1998; 44:H1898-H1904.

102. Shila Jalali, Yi-Shuan Li, Mohammad Sotoudeh, et.al. Arterioscler Thromb Vasc Biol. 1998; 18:227-234.

103. Young-Mi Go, Heonyong Park, Matthew C. Maland, et.al. Am J. Physiol Heart Circ Physiol. 1998; 275:1898-1904.

104. Kevin Janes, et.al. Science. 2005; 310: 1646-1653.

105. Assefa, Z., M. Garmyn, R. Bouillon, W. Merlevede, J. R. Vandenheede, and P. Agostinis. J. Invest. Dermatol. 1997; 108:886-891.

106. Derijard, B., M. Hibi, I. H. Wu, T. Barrett, B. Su, T. Deng, M. Karin, and R. J. Davis. Cell. 1994; 76:1025-1037.

107. Liu, Z. G., H. Hsu, D. V. Goeddel, and M. Karin. Cell. 1996; 87:565-576.

108. Lo, Y. C., J. S. Wong, and T. F. Cruz. J. Biol. Chem. 1996; 271:15703-15707.

109. Luo, Y., H. Umegaki, X. Wang, R. Abe, and G. S. Roth. J. Biol. Chem. 1998; 273:3756-3764.

110. Li, S., M. Kim, Y. L. Hu, S. Jalali, D. D. Schlaepfer, T. Hunter, S. Chien, and J. Y. Shyy. J. Biol. Chem. 1997; 272:30455-30462.

111. Jo, H., K. Sipos, Y. M. Go, R. Law, J. Rong, and J. M. McDonald. J. Biol. Chem. 1997; 272:1395-1401.

112. James Surapisitchat, Ryan J. Hoefen, Xinchun Pi, and et al. PNAS. 2001; 98: 6476-6481.

113. Davies PF. Physiol. Rev. 1995; 75: 519-560.

114. Kevin Janes, et.al. Science. 2005; 310: 1646-1653.

115. Dower, S.K., and Qwarnstrom, E.E.. Bioch. Soc. Trans. 2003; 31:1463-1467.

116. Fiering, S., Northrop, J.P., Nolan, G.P., Mattila, P.S., Crabtree, G.R., and Herzenberg, L.A.. Genes Dev. 1990; 4:1823-1834.

117. Fiering, S., Whitelaw, E., and Martin, D.I.K.. BioEssays. 2002; 22:381-387.

118. Hume, D. A. Blood. 2002; 96:2323-2328.

119. Ko,M.S. BioEssays. 1992; 14:341-346.

120. Nair, V.D., Yuen, T., Olanow, C.W., and Sealfon, S.C.. J. Biol. Chem. 2004; 279:27494-27501.

121. Haralick, R. M. and Shapiro, L. G. Computer Vision, Graphics, Image Process. 1985; 29:100-132.

122. Ridler, T. and Galvard, S. IEEE Transactions on System. 1978; 8: 630-632.

123. Thiran J. and Macq B. IEEE Transactions on biomedical engineering. 1996; 43: 1011-1020.

124. Fang B., Hsu W., and Lee M. IEEE Transactions on nanobioscience. 2003; 2: 94-103.

125. Zhao P., Mao K., and Tan P. IEEE EMBS Asian-Pacific Conference on Biomedical Engineering. 2003; 168-169.

126. Petushi S., Katsinis C., Coward C., et al. IEEE International Symposium on biomedical imaging: Macro to Nano. 2004; 1: 424-427.

127. Raser, J.M., and O'Shea, E.K. Science.2004; 304:1811-1814.

128. Elowitz, M. B., Levine, A.J., Siggia, E.D., vvand Swain, P.S. Science. 2002; 297:1883-1886.

129. Hoffmann, A., Levchenko, A., Scott, M.L., and Baltimore D. Science. 2002; 298: 1241-1245.

130. Nelson, G., See, V., Horton, C.A., Spiller, D.G., Edwards, S.W., McDowell, H.P., Unitt, J.F., Sullivan, E., Grimley, R., Benson, N., Broomhead, D., Kell, D.B., and White M.R.H. Science. 2004; 306: 704-708.